CONF-8603109--3

BNL--37795

DE86 010547

2/27/86
Presented at Fourth European Symposium on
Semiconductor Detectors, Munich, W. Germany, 3/3-5/86;
Submitted to IEEE Transactions on Medical Imaging

Proposal for a New Tomographic Device Providing Information on the Chemical Properties of a Body Section*

Emilio Gatti† and Pavel Rehak
Brookhaven National Laboratory, Upton, NY 11973

Josef Kemmer
Faculty of Physics
Munich Technical University, D-8048 Garching, W. Germany

Abstract

A system to analyze the chemical properties of a region of tissue located deep inside the human body without having to access it is proposed. The method is based on a high precision detection of X-rays or γ-rays (photons) from an external source Compton scattered from the tissue under inspection. The method provides chemical information of plane regions lying not too deep inside the body (<6 cm). The amount of radiation absorbed by the body is about the same as needed for a standard X-ray tomography. The exposure time is estimated to be shorter than 10 minutes.

*This research has been supported by the U.S. Department of Energy under Contract DE-AC02-76CH00016.
†Permanent address: Istituto di Fisica, Politecnico di Milano, 32-Piazza Leonardo da Vinci, Milano, Italy.

I. Introduction

The ability to view clearly a section within a human body, without interference from other regions, has long been a goal of medical radiology. In 1968, Hounsfield [1,2] developed a technique known as Computer-Assisted Tomography which produced striking cross-sectional images of the human head in a run time of a few minutes with a dose of few rad to the tissue. This advance has revolutionized much of medical radiography and stimulated development of other imaging techniques. Among them the Nuclear Magnetic Resonance [3] imaging technique looks very promising today mainly because it does not introduce any ionizing radiation into the patient's body. It measures the density plus relaxation times of the hydrogen instead of the total density which is measured by a standard tomography, thus providing additional medical information. In fact, almost all existing imaging methods measure different entities and are more complementary than in competition with one another [4].

The proposed method reconstructs the elemental composition and some chemical bonds among different atoms in an imaging plane or in a volume element. The potential of this method for medical diagnosis is self evident. Detection of density and chemical changes in coronary and cerebral arteries due to arteriosclerosis may be the most important and immediate diagnostic application of the proposed method. According to the authors knowledge no other method exists which can provide similar information.

The proposed method is based on analysis of the Compton profile of X-rays or γ-rays (photons) incoherently scattered on electrons within the imaging plane. It will be shown later that the shape of

the Compton profile is related to the momentum distribution of electrons on which the photons were scattered. The Compton profile is known for each element, thus it serves as a "fingerprint" to identify the elemental composition of the matter in the viewing section. Moreover, the shape of the Compton profile is sensitive to the state of the valence electrons of the atoms. Therefore a careful analysis of the Compton profile reveals also some information about the molecular structure.

In Section II the principles of the method are discussed. Section III is dedicated to the description of a new germanium high resolution (energy and position) detector which is the central part of the new tomographic system. The detector's high acceptance allows application of the Compton profile method, up to now a rare laboratory tool, to a much wider field.

Section IV studies the practical aspects and the limitations of the method. The principal limitation is due to the statistical accuracy of the data closely connected to the radiation dose absorbed within the patient's body.

II. Principles of the Method

We will start our studies by first considering the Compton scattering from a selected point, practically from a small volume fixed within the living body. This is the key to the elemental analysis. Then we will extend the ideas to the analysis of a line and to a full tomographic plane.

A. Compton Scattering

Fig. 1a shows one of possible apparata to provide the elemental analysis of the patient's tissue. A well collimated pencil beam of monoenergetic photons enters almost perpendicularly the person's steady head. A high resolution germanium detector covers a large area around the photon beam. The detector measures the energy and the impact point of photons scattered backwards into a large solid angle by the patient's tissue.

Fig. 1b shows the cross sections of two collimators. The fluorescenceless lamellas of the first collimator are placed radially relative to the pencil beam. Ideally these lamellas do not prevent photons coming from the beam line to reach the detector. They, however, prevent a large part of photons which were scattered more than once within the tissue, from reaching the germanium detector. The lamellas of the second collimator are placed in such a way that only photons scattered from a preselected part of the primary beam line are allowed to enter the detector. The lamellas also suppress multiple scattered photons from reaching the detector. Effectively these two collimators define a point deep within the patient's tissue from where single scattered photons are measured in the high resolution detector, while photons scattered somewhere else or multiple scattered photons are prevented from reaching the detector.

We now address the physics of the photon scattering within the patient's body. The Compton scattering is the incoherent scattering

of photons on electrons. It is one of the fundamental interactions of photons with matter. For the light elements which form the human tissue (the atomic number of its elements run from Z=1, to about 15) and for photon energies in the 50 to 2000 keV region, Compton scattering is also the most likely photon interaction. We will choose our photon energy within the region where the Compton scattering dominates the total photon attenuation coefficient (≈90%) in human tissue [5] and neglect the other photon processes in the tissue, since they are not detected in the proposed apparatus.

The well known Compton formula [6] relates the energy of a scattered photon $\omega_2^{(o)}$ to the photon scatter angle θ (Fig. 2a).

$$\omega_2^{(o)} = \frac{\omega_1}{1 + \delta\ (1-\cos\theta)}\ ;\ \delta = \frac{\omega_1}{mc^2} \qquad (1)$$

where ω_1 is the energy of the incident photon, m is the electron mass and c is the velocity of light in vacuum. The derivation of formula (1) assumes that the photon was scattered from a free electron at rest. The Compton formula (1) predicts for a given scatter angle θ a well defined value of the energy of the scattered photon $\omega_2^{(o)}$. Detecting the photons at one angle we should measure the same energy for all photons. In reality this is not the case. The peak of the energy spectrum of photons scattered at a given angle has an intrinsic width as shown in Fig. 3.

The broadening of energy distribution of the scattered photons was known as early as 1929 [7]. The reason for the broadening is the initial state of electrons in real materials. Electrons are not free and not at rest. Anticipating the results of the following analysis we can say that the amount and the shape of the broadening reflects how electrons are bound within the matter, that is, it depends on the atomic composition of the material. Each element broadens the energy distribution in its characteristic way which is the "fingerprint" mentioned in the Introduction.

B. Compton Profile and Electron Momentum Distribution

The rigorous analysis of the Compton scattering from bound electrons was performed by Eisenberger and Reed [9] and Ribberfors [10] in a general relativistic case. Their work confirmed the validity of the impulse approximation (IA) method to analyze the scattering. The IA method was used already be DuMond [7] to show that the distribution of electron momenta in Beryllium was consistent with the new Fermi statistics and not with the classical Maxwell-Boltzmann distribution law. In IA the Compton scattering from bound electrons is equivalent to the photon scattering from free but non-stationary electrons. The interaction is depicted in Fig. 2b. The next result is the break-down of Equation (1) due to the initial electron momentum $\vec{p}_1$. The difference between the energy of the scattered photon in IA ω_2 and the energy of the scattered

photon $\omega_2^{(o)}$ on an electron at rest is given by

$$\Delta\omega = \omega_2 - \omega_2'^{(o)} = \frac{p_z \cdot \left|\vec{k}\right|}{m \cdot \left(1+\delta\ (1-\cos\theta)\right)} = \frac{p_z}{m} \cdot \left|\vec{k}\right| \cdot \frac{\omega_2^{(o)}}{\omega_1} \qquad (2)$$

where p_z is the component of the initial electron momentum p_1 along the Z-axis which was defined as being with the opposite orientation parallel to the vector of photon momentum transfer $\vec{k} = \vec{k}_1 - \vec{k}_2$; m,$\theta$ and δ retain their previous meaning. Formula (2) is a direct consequence of the relativistic kinematics of the scattering process. The only assumption in its derivation was that the initial kinetic energy of the scattering electron is much smaller than the total electron energy at rest (511 keV). This assumption holds well for electrons of light elements present in human tissue.

Equation (2) shows that the energy of the scattered photon at a given angle depends on the projection of the initial electron momentum. Roughly speaking, the measurement of the distribution of $\Delta\omega$ is $\left|\vec{k}\right| \cdot \omega_2(o)/(m \cdot \omega_1)$ multiplied by the distribution of projected initial momentum p_z, which is called the Compton profile $J(p_z)$. From the first principles of quantum mechanics we can write the Compton profile as

$$\begin{aligned} J(p_z) &= \int_{p_x}\int_{p_y} N(p_x,p_y,p_z)\,dp_x\,dp_y \\ &= \int_{p_x}\int_{p_y} \chi^*(\vec{p}) \cdot \chi(\vec{p})\,dp_x\,dp_y \end{aligned} \qquad (3)$$

where $N(p_x,p_y,p_z) = N(\vec{p})$ is the density momentum distribution which was expressed by the electron momentum wavefunction $\chi(\vec{p})$. The momentum wavefunction $\chi(\vec{p})$ is a Fourier-Dirac transformation of the more familiar spatial wavefunction $\phi(\chi)$; both satisfy the same Schrödinger equation. There is also a more direct connection between the Compton profile $J(p_z)$ and the spatial wavefunction $\phi(\chi)$[11]. In recent years the study of the Compton profile emerged as a practical tool for studying electronic structure of solids, liquids and gases. Excellent reviews of the topic are available [12-15].

For our purpose it is sufficient to know that each element has its own Compton profile.

Compton profiles were calculated for all elements. Calculations based on Hartree-Fock wavefunctions are tabulated [16] and agree very well with the measurements. Figure 4 from reference [8] shows the degree of the agreement for a helium atom.

Figure 5 shows calculated Compton profiles for biologically important atoms of hydrogen, carbon and sodium normalized to 1 electron [16]. The difference of the shapes of the Compton profile of individual elements is the principle of the elemental analysis. The observed Compton profile is almost the weighted sum of the Compton profiles of the individual elements. The problem of elemental analysis is reduced to the decomposition of the experimental distribution as a sum of known elemental distributions.

However, the method has a greater potential. The Compton profile is sensitive to the state of valence electrons of atoms which combine to form molecules. Equation (3) shows the relation of the Compton profile with the electronic momentum wave function. The momentum and the position wave functions form a Fourier transform pair. Consequently the outermost electrons which form chemical bonds and are spatially spread out, are localized in the momentum space giving narrow contribution to the Compton profile.

Figure 6 shows the experimental confirmation of the effect of hemical bonds on the Compton profile (taken from Ref.[17]). The authors plotted the measured Compton profiles for atomic carbon, diamond and the C-C bond in ethane gas which has the same length as the C-C bond in diamond (1.54 Å). In the ethane molecule and diamond, the effect of the increased localization of electrons in bands compared to atomic carbon is dramatic. It causes a decrease of J(q) at q = 0 and a large increase for q between .6 and 1.8 atomic units.

More studies of the chemical bonds were published [18]. All w e riented towards basic research. Today it is still too difficult to foresee which feature of the analysis has the largest importance for diagnosis.

Before closing this part let us outline the method of measurement of the Compton profile with a large area germanium detector. In a standard method the secondary photons scattered only at a given angle reach the detector. Their energy spectrum is practically the Compton profile.

In the proposed method the photons scattered within a large solid angle are accepted in the detector. The detector provides the energy and the position in the detector of each individual photon. The scattered angle Θ is determined from the position of the photon in the detector. Knowing the scattered angle, the ideal Compton energy $\omega_2^{(o)}$ is calculated (Equation (1)). The difference between measured and calculated energies $\omega_2 - \omega_2^{(o)}$ is related to the projection of the initial electron momentum p_z according to Equation (2). Calculating p_z for each detected photon we obtain the distribution of p_z which is almost the Compton profile $J(p_z)$. To be more rigorous we may correct our profile by a small and slowly varying factor which takes into account the variation of the Compton cross section on p_z and other factors [9,10]. It may turn out that for our purpose, that is to discriminate among the Compton profiles of different elements, these corrections are not necessary.

C. Elemental Analysis in a Tomographical Plane

Let us remove the second collimator (Fig. 1b) from the apparatus. The function of this collimator was to select a given region along the primary beam line for the Compton profile analysis. In a new modified apparatus primary photons scattered anywhere along the beam line may reach the detector and be measured there. This alternative apparatus is shown in Fig. 7a. Here the germanium detector covers a large solid angle around 90° relative to the primary monoenergetic photon beam. The fluorescenceless collimator lamellas shown in Fig. 7b prevent a large part of multiply scattered photons from reaching the detector. There is no collimator in the other

direction and photons scattered anywhere along the beam may reach the detector. Note that these two detector positions relative to the direction of the primary beam are not mutually exclusive. We can analyze the Compton scattering by two sets of detectors at the same time.

To gain an insight into the analysis of the Compton scattering along the beam line let us for the moment disregard the effect of electron bonds on the scattering. That means that the Compton profile is a δ-function and we have a one-to-one relationship between the energy of the scattered photon $\omega_2^{(o)}$ and the scattered angle θ (Equation (1)). The knowledge of the energy $\omega_2^{(o)}$ gives the scatter angle θ and from the position of the measured photon in the detector we can unambiguously determine the position along the beam where the photon was scattered (Fig. 7c). The frequency of scattered events in the tissue depends on the electron density at that position. We see that the energy and the position of the scattered photons provides the electron density along the primary photon beam line. Moving the beam together with the detectors the electron density from a set of lines defining effectively a plane, can be obtained. In the language of Transmission Tomography one view only is enough to obtain a full density picture.

We would like to stress the difference between the described method and the traditional Compton scattering tomography. The use of Compton scattered photons for diagnostic imaging was pioneered by Lale [34] and by Clarke [35]. A relatively recent overall appraisal of traditional Compton scatter imaging methods was published in 1981

[36]. All of the traditional methods localize the scattering position by means of narrow angular collimators. Therefore the acceptance angle to detect scattered photons is small and in direct conflict with the attainable position resolution. A crude (±10%) energy measurement is sometimes performed. The energy is used only to reject the multiple scattered events. The process described herein uses the energy of the scattered photon instead of collimators to localize the position of the scattering center. The acceptance is consequently larger by a factor roughly equal to the number of collimators along the primary beam direction in a traditional method (≈100 times).

The differential cross section for the compton process is given by Klein-Nishina formula [37] which for an unpolarized primary beam can be written

$$\frac{d\sigma}{d\Omega} = \frac{1}{2} r_o^2 \cdot y^2 \left(\frac{1}{y} + y - \sin^2\theta\right) \qquad (4)$$

where the parameter y is also a function of θ,

$$y = \frac{1}{1 + \delta(1-\cos\theta)} \qquad (4a)$$

r_o is the classical electron radius (=2.818x10^{-15} m), θ and δ

retain their meaning from Equation (1). The differential cross section $d\sigma/d\Omega$ is the probability that an incident primary photon will be scattered into a unit solid angle at the polar angle θ by a density of scattering centers of 1 electron per cm^2. Fig. 8 shows the calculated Klein-Nishina cross section for the energy of primary photons of 159 keV. In our case it means that photons scattered from a small volume element are distributed in the detector according to Formula (4). This constraint is unimportant for the case under consideration of photon scattering on free electrons at rest, but it plays a central role in elemental analysis from photons scattered by real electrons.

Before investigating the method's modification necessary to include real electrons, let us evaluate the precision of the position of the scatter center determined from the energy measurement. Differentiating Eq. (1) with respect to θ we obtain

$$\Delta\theta = \frac{mc^2}{\sin\theta \cdot \omega_2^{(o)}} \quad \frac{\Delta\omega_2^{(o)}}{\omega_2^{(o)}} \qquad (5)$$

For a relative energy resolution $\Delta\omega_2(o)/\omega_2(o)$ of .2% at $\omega_2(o)$ = 100 keV, the angular resolution at 90° is 10^{-2}rad. For a detector-beam distance of 10 cm the position resolution is 1 mm.

The effect of electron motion and binding as discussed in Part B can be summarized in the following formula for the double differential cross section

$$\frac{d^2\sigma}{d\omega_2 d\Omega} = \frac{d\sigma}{d\Omega}_{KN} \cdot \frac{m\,\omega_1}{|\vec{k}| \cdot \omega_2^{(o)}} \cdot J'(p_z) \qquad (6)$$

where $(d\sigma/d\Omega)_{KN}$ in the Klein-Nishina cross section defined in Equations (4), m, ω_1, $\omega_2^{(o)}$ and k retain their previous meaning. $J'(p_z)$ is almost the Compton profile $J(p_z)$ defined in Equations (3). We have made the same approximations as in Part B and $J'(p_z)$ is not exactly the Compton profile $J(p_z)$ but it is still a well defined property of scattering atoms. The relation between the Z-component of the momentum of the electron and the energy of the secondary photon used in deriving (6) was given in Equation (2).

The double differential cross section $d^2\sigma/d\omega_2 d\Omega$ is an extension of the previously defined differential cross section $d\sigma/d\Omega$. It includes the requirement that the energy of the scattered photon is in a unit energy interval at the energy ω_2. For a moment let us assume that we measure in the germanium detector the position and the energy only of photons scattered at a given point, P, along the primary beam. The distance of the point P from the collimator is X

as indicated in Fig. 7c. The scattering angle Θ is thus known by the measurement of the position P' of the scattered photon in the detector and the known beam-detector distance D. If there are $n_e(x)$ electrons per unit volume at the point P within the tissue the number of detected photons with the energy in an interval $(\omega_2, \omega_2+\Delta\omega_2)$ and in a surface element of the detector i is

$$N_x(i,\omega_2)\Delta\omega_2 \cdot \Delta x = g(i,x) \cdot E(i,x,\omega_2) a(i,x,\omega_2) \cdot \phi(x) \cdot n_e(x) \cdot \frac{d^2\sigma}{d\omega_2 d\Omega} \cdot \Delta\omega_2 \Delta x \tag{7}$$

where $g(i,x)$ is a purely geometrical factor which "converts" the combinations of i and x into Θ, $E(i,x,\omega_2)$ is the detector efficiency, $a(i,x,\omega_2)$ is the attenuation factor of scattered photons and $\phi(x)$ is the integrated flux of primary photons at x. The double differential cross section in Equation (7) can also be expressed by x,i and ω_2.

$$\frac{d^2\sigma}{d\omega_2 \cdot d\Omega} = C_{KN}(i,x) \cdot \frac{m\,\omega_1}{|\vec{k}| \cdot \omega_2^{(o)}} \cdot J_x'(p_z) \tag{8}$$

We substitute (8) into (7) and obtain

$$N_x(i,\omega_2)\Delta\omega_2 \cdot \Delta x = F_{KN}(i,x,\omega_2) \times n_e(x) \cdot \Delta x \cdot J'_x(p_z) \cdot \Delta p_z \qquad (9)$$

where $F_{KN}(i,x,\omega_2) = g(i,x) \cdot E(i,x,\omega_2) \cdot a(i,x,\omega_2) \cdot C_{KN}(i,x)$ (10)

and Δp_z stands for $\Delta\omega_2 \cdot m\omega_1 / \left(\left|\vec{k}\right| \cdot \omega_2^{(o)} \right)$. According to the spirit of our elemental analysis the product of the total electron density and the Compton profile at the point x can be decomposed into individual contributions and written

$$n_e(x) \cdot J'_x(p_z) = \sum_Z n_e^{(Z)}(x) J'(p_z,Z) \qquad (11)$$

where the summation is over all relevant elements with the atomic number Z. The $n_e^{(Z)}(x)$ is the electron density of the element with the atomic number Z at the point x; $J'(p_z,Z)$ are the known elemental "Compton profiles" [16]. p_z in $J'(p_z,Z)$ can also be expressed as a function of x,i and ω_2

$$J'(p_z,Z) = J''(x,i,\omega_2,Z) \quad . \tag{12}$$

Substituting (12) and (11) into (9) we obtain

$$N_x(i,\omega_2)\Delta\omega_2 \cdot \Delta x = F_{KN}(i,x,\omega_2) \cdot \Delta x \sum_Z J''(x,i,\omega_2,Z) \cdot n_e^{(Z)}(x) \cdot \Delta p_z \tag{13}$$

Up to now we have assumed that photons were scattered from the vicinity of a given point P. Equation (13) describes therefore the method of elemental analysis from a small volume around the point P in a mathematical form suitable for computer programming. This equation summarizes the physics described at the end of Part 1B. Equation (13), however, shows explicitly corrections due to detector efficiency, attenuation, etc.

In a tomographic application the detector sees the scattered photons from all points along the primary beam line. The measured distribution is therefore

$$N(i,\omega_2)\Delta\omega_2 = \sum_{\Delta x} N_x(i,\omega_2)\Delta\omega_2 \cdot \Delta x$$

or

$$N(i,\omega_2)\Delta\omega_2 = \sum_{\Delta x} \Delta x \cdot F(i,x,\omega_2) \cdot \Sigma J''(x,i,\omega_2,Z) \cdot \Delta p_z \cdot n_e^{(Z)}(x) \tag{14}$$

This formula can be interpreted as a system of linear equations for each i and ω_2 with $n_e^{(Z)}(x)$ as unknown parameters. The solution of the system (14) gives the elemental composition at each point along the beam line.

The solution of the system (14) must be understood in the statistical sense of a "best estimate" of $n_e^{(Z)}(x)$. The measured distribution is subject to well known statistical fluctuations which propagate to the solution. The number of equations in the system (14) is larger than the number of unknown. The exact solution generally does not exist. The statistical solution of our problem is a set of $n_e^{(Z)}(x)$ which minimizes an appropriate χ^2 estimator.

The knowledge of $n_e^{(Z)}(x)$ gives us the elemental composition and density of the tissue along the beam line. By moving the apparatus the chemical composition of a plane can be obtained.

III. Germanium High Resolution Detector

The measurement of a Compton profile used to be a time consuming experiment. Before the application of Ge(Li) detectors in 1972 by Eisenberger and Reed [19] a crystal diffraction spectrometer was generally used to measure the energy of scattered photons. Each point of a Compton profile had to be measured individually in time. To determine a Compton profile about 300 points were typically measured. Eisenberger and Reed speeded up the measuring time by about the same factor of 300 by using an energy sensitive Ge detector which measured all the points at once. They did not have a position sensitive detector and had to define the scattering angle by a small entrance hole in front of the Ge-detector with an angular acceptance of 5×10^{-4} steradians.

The proposed method uses a position sensing Ge detector and removes the limitations of a small angular acceptance. Angular acceptance can be as large as 1 steradian which decreases the exposure time and the radiation dose by a factor of a thousand. The measurement time decreases from typically 3 days to 5 minutes. This time is reasonable for a practical diagnosis.

The Ge detector which measured the energy and the position of photons with high precision is based on a new charge transport scheme in semiconductor detectors [20-22], (US - patent pending). The detection process can be approximately divided into three steps.

i) Photon conversion and creation of electron-hole pairs.

ii) Transport of electrons from the conversion point to the low capacitance anode.

iii) Signal charge measurement on the anode.

The first step depends only on the detector material and is the same as in a standard Ge detector. The improvement of measurement is due to the second and the third steps.

In the first step the photon interacts by a photo-effect within the detector and a part of its energy is used to create electron-hole pairs. The number of created pairs is strictly proportional to the photon energy. The fluctuations in the number of created pairs limits the precision of the photon energy measurements. The attainable energy resolution σ_ω is proportional to the statistical spread in the number of generated charges [23].

$$\sigma_\omega = \sqrt{\omega \cdot w \cdot F} \qquad (15)$$

where σ_ω is the root mean square (r.m.s.) of the energy measurement; ω is the photon energy, w is the energy needed to create one electron-hole pair (=2.96 eV) and F is the Fano factor (≈.1 for a good detector). For ω = 100 keV the σ_ω is 180 eV or about 0.2% as was used in equation 5.

It will be shown later that the precision of the photon energy measurement is the most important part of the proposed method for the elemental analysis. The remaining two steps in the detection process thus must not compromise the energy resolution given by Equation 15.

The second step of the detection process is the transport of signal electrons. Figure 9a shows schematically the movement of electrons within the detector from the impact point of the photon towards the anode. For most of their journey the electrons are moving in a controlled way parallel to the detector's faces. This movement is used to measure the impact position of the photon in the detector.

We are going to consider the electron movement and the electric potential causing it in some detail. Fig. 9b shows the negative electric potential (potential energy of electron) within the detector. The shown potential is the result of the superposition of potentials of two electric fields. The first field is due to the uniform density of the positive charges bound in the Ge crystal lattice after all mobile charges were swept away (depleted material). The second field parallel to the detector faces was applied externally to transport electrons towards the anode. The potential shown in Fig. 9b is produced in an n-doped bulk semiconductor which has rectifying junctions on its faces. Rectifying junctions are held at the appropriate potential through connections to a voltage divider. The anode (shown in Fig. 9a only) is a back contact of small area located close to the edge of the detector.

The travel time of electrons inside the semiconductor detector measures the distance of the photon conversion from the anode. During the travel (drift) time the electron charge is screened by the rectifying junctions and the signal appears only when the electrons arrive close to the collecting anode [20].

A • ilar detector, called semiconductor drift chamber, was already built and tested [21,22]. The detector was made out of silicon and it is mainly intended to measure the ɾɔsition of charged particles in elementary particle physics experiments.

The performance of the prototype detector confirmed the validity of the underlying mechanism of the charge transport in fully depleted semiconductor detectors. The position resolution was better than 5 μm for a tested drift distance up to 4 mm (Fig. 10).

An independent measurement of photon energies at room temperature gave an estimate of electron trapping effects of .0 ± .2% at 5 mm long drift.

The Lawrence Berkeley Laboratory semiconductor detector division has built a germanium detector based on a similar idea [24]. The drift field was generated by the gradient of the density of the electrically active impurities in the germanium crystal. The continuous rectifying junctions were implanted on both faces of the detector (Fig. 11). The reported position resolution was better than .5 mm for the drift distances up to 3 cm.

At a very low temperature (≈ 77°K) a trapping of signal electrons was seen. The amount of electron trapping decreased rapidly with temperature. It was found to be almost negligible at 120°K.

The position sensing method described above by measuring the drift time of electrons in the detectors gives only one coordinate. The knowledge of one coordinate is sufficient to provide the elemental analysis of a small volume inside the human body (Fig. 1).

To obtain the elemental composition of a tomographic plane the knowledge of both coordinates is required.

A fully depleted thick germanium charge coupled device (CCD) offers the possibility to perform the photon detection in two dimensions. The description of a fully depleted CCD can be found in Ref. 20. The charge is transported by the action of a peristaltic pump as in a standard CCD. The major difference between the proposed and a standard CCD is the thickness of the active region for the photon detection (depleted region). The standard CCD has typically a depletion region of 10 μm thickness. The proposed fully depleted CCD will have a fully active thickness of a few mm.

A fully depleted CCD has not yet been built. However, the existence of standard CCD and a very good performance of new detectors based on the same principles as a fully depleted CCD gives us confidence that our analysis of a fully depleted CCD is correct.

The third step in the detection process is the charge measurement. A direct consequence of our new charge transport scheme is the very small capacitance (electrical) of the collecting anode. Moreover, this capacitance is independent of the detector surface area. Each of the considered detectors is a large area detector with a very small collecting anode capacitance. Small anode capacitance helps to decrease the electrical noise. The signal voltage U_s at the preamplifier input is the ratio of the signal charge Q_s and the total capacitance C_T ; $U_s = Q_s/C_T$. A small capacitance leads to a large signal voltage which makes the noise of the preamplifier less important. More precisely, the smaller input

capacitance allows the signal processing circuits to use more bandwidth and increase the rate capability of the system.

Assuming that the detector leakage current and all other sources of parallel noise are sufficiently small, the equivalent noise charge (ENC) can be expressed as [25,26]

$$ENC = C_T\sqrt{e_n^2}/\sqrt{T} \qquad (16)$$

where e_n^2 is the series voltage noise (spectral density) of the input field effect transistor (FET) C_T - is the total input capacitance and T is the peaking time of the final waveform at the output of the main amplifier. A commercially available FET 2N4416 has $\sqrt{e_n^2} \approx 1.5$ nV/$\sqrt{\text{Hz}}$ and input capacitance of 2.5 pF. If we assume the anode capacitance to be also about 2.5 pF and the peaking time of 4 μs the ENC from Equation (16) is 24 electrons. The equivalent noise energy is 24 electrons x 2.96 eV/electrons ≈ 70 eV. The total line width (r.m.s.) is then $\sqrt{70^2 + 180^2} \approx 195$ eV. We can see that the loss of energy resolution due to the electrical noise is only 8%, compared to the natural width of 180 eV given by Eq. (15).

To conclude this part we can say that the principles of photon detection with high precision of energy and position measurements are well understood and demonstrated. However, the test devices were realized mainly in silicon instead of germanium. The proposed method requires very reliable germanium detectors. The application of planar technology used to build silicon detectors into germanium may be the most demanding part of the project.

IV. Practical Aspects and Limitations of the Method

The analysis in this section is limited to the study of the elemental composition of a selected small region within the human body.

We are going to address the most important question, that of the radiation dose absorbed by the patient's tissue during exposure time. The proposed method as explained in Section II is based on the Compton profile measurement. In recent years several apparata for accurate Compton profile measurements for basic research in physics and chemistry were constructed [27-30]. A large part of our analysis in this section will be based on the referenced Compton profile work.

A. Choice of the Incident Photon Energy

The dotted line in Fig. 12 shows the line broadening of the Compton profile measurement in atomic units due to the energy resolution of the germanium detector as a function of the incident photon energy. We could obtain the same curve by combining Equation (15) which gives the energy resolution of the germanium detector and Equation (2) which describes the kinematics of the process under study. We see a rapid improvement of the resolution with the energy of incident photons up to 100 keV. Then there is a slower improvement up to about 250 keV and practically no improvement above this energy level.

The arrows in Fig. 12 indicate energies typically used for Compton profile experiments. We are going to show that the arrow at 159.0 keV which corresponds to a ^{123m}Te γ-ray source is close enough to the optimum value for the energy of primary photons.

Using primary photons of 159 keV from Equation (1) we obtain 98 keV for the energy of secondary back scattered photons ($\theta \approx 180°$). For these energies incident and scattered photons interact inside the human body mainly through the Compton scattering process and the mean attenuation length in the tissue is 6.5 and 6.0 cm, respectively. This relatively long value of the photon attenuation length is important for the analysis deeper within the body.

On the other hand, 98 keV energy of scattered photon is low enough to interact in the germanium detector mainly through the photo-effect process. A photon interacting through the photo-effect process within the photon detector deposits all its energy in the immediate vicinity of the interaction. This feature of the photon interaction is used to measure the photon position. A Compton scattering of the photon in the detector followed by a photo-effect far away from the original interaction may lead to an incorrect position measurement and contribute to the background. We plan to analyze the signal waveforms at the anode and reject a large part of this background. The correct choice of the photon energy already makes the probability of this background low.

The importance of the photo-effect interaction in the detector for the position measurement excludes the use of silicon as a material for detectors. Photo-effect cross section increases with the fifth power of the atomic number. A low atomic number of silicon (Z=14) gives an unacceptably low photo-effect cross section.

The linear photo-absorption coefficient in germanium for a photon energy of 98 keV is about 2 cm^{-1} [31]. A 3mm thick germanium detector would have a detection efficiency of about 50%.

Dependence of the radiation dose on the photon energy will be discussed in Part C. There are two additional reasons for choosing this value for the photon energy. The source of this energy is not too difficult to shield and it is easy to prepare a desirable beam by simple collimation. And finally, the photon energies are below the threshold for radiation damage of the germanium detectors [32].

B. Geometry of the Incident Photon Beam

Solid lines in Fig. 12 show the line broadening of the Compton profile measurement due to the error in determination of the scattering angle θ for three different values of θ. The assumed error of the scattering angle has FWHM of 2 degrees. The resolution's insensitivity to the exact knowledge of the scattering angle for large θ justifies the use of backscattering for the measurment (Fig. 1). To cover a large enough solid angle we may want to include all angles down to 150 degrees. From the solid line for θ = 150° in Fig. 12 we see that at ω_1 = 159 keV the error in the

Compton profile measurement due to a 2 degree error in the determination of θ is 75% of the error due to the energy measurement (Dotted line in Fig. 12). By summing these two errors in quadrature, the broadening of the Compton line would be 25% compared to the width due to the energy resolution only. We have to keep the angular error at 1.5 degrees to obtain a broadening below 15% for all scattering angles from 180° down to 150 degrees. The acceptance angle of the apparatus is .84 steradians.

The error in scattering angle is due to the following three causes: (Fig. 13) i) the incident beam divergence, ii) the transverse beam dimensions, and iii) the position resolution of the germanium detector. We will keep errors due to the beam divergence and the position resolution of the detector small and use a relatively large beam size to minimize the radiation dose. From Fig. 13 we can easily find the angular error $\Delta\alpha = \alpha - \alpha'$ due to the transverse dimensions of the beam d:

$$d = \Delta\alpha \cdot R \qquad (17)$$

where R is the distance between the scattering center and the detector. Taking R = 10 cm, the transverse beam dimension is 2.7mm. The volume element under study is thus a cylinder with a diameter of about 3mm and with a height of 6mm. The axis of the cylinder is in the direction of the incident beam (Fig. 13).

C. Radiation Dose

P. Eisenberger and W.A. Reed [19] detected about 10^6 backscattered photons to obtain a precise measurement of the Compton profile of Krypton. In Appendix I it is shown that 10^6 counts is also a sufficient statistical sample for our elemental analysis. We are going to calculate how many primary photons have to enter the human body to detect these 10^6 scattered photons and how large the dose is to the skin.

In the first approximation the number of detected photons N_D is

$$N_D = N_{in} \cdot A_{in} \cdot Sc_D \cdot A_{sc} \cdot \varepsilon_{det} \qquad (18)$$

where N_{in} is the number of incident photons, $A_{in}(A_{sc})$ the attenuation of the incident (scattered) photons, Sc_D is the probability of a Compton scattering into the solid angle covered by the detector within the volume element under study and ε_{det} is the detection efficiency.

The probability of the useful Compton scattering can be estimated from the Klein-Nishina cross section (Fig. 8). For our region of scattering angles ($5/6\pi$-π), the section is practically constant and equal to .033 barn/electron/sterad. The probability Sc_D can be expressed as

$$Sc_D = \frac{d\sigma}{d\Omega} \cdot \Omega \cdot n_e \cdot h$$

where Ω is the solid angle covered by the detector (.84)

n_e is the electron density in human tissue (3.35×10^{23} el/cm^3)

h is the height of the cylinder under investigation (.6cm)

Substituting the numerical values, we obtain Sc_D = .56%. If we assume that the volume under study is located 6cm deep inside the human body, $A_{in} \approx A_{sc} \approx 1/e$, we obtain from Equation (18) the number of incident photons as $N_{in} = 2.6 \times 10^9$ where ε_D was taken to be 50%.

The dose D_0 in rads to the skin is given by

$$D_0 = \frac{\mu_{en} \cdot \omega_1 \cdot N_{in}}{100 \cdot \frac{\pi}{4} \cdot d^2 \cdot \rho} \tag{19}$$

where μ_{en} is the energy absorption coefficient in cm^{-1}, ρ the density of the human tissue in g/cm^3, ω_1 the photon energy in ergs and d the effective diameter of the incident beam in cm. The factor of 100 in the denominator converts from ergs/g to rads since 1 rad is 100 erg/g. Taking the density equal to 1 g/cm^3, μ_{en} equal to .024 cm^{-1} and all other quantities as calculated above the dose to the skin is 2.3 rads. The dose given to a patient in a scan by a standard X-ray tomography is 2.5 rad. [33]. The radiation dose received by the skin can be reduced using the sweeping beam technique. The beam, while being kept focussed on the volume element, is moved in a sweeping motion on the skin's surface. The incident beam is spread over a larger skin area and the dose to the skin can be substantially reduced. With this technique it is the volume under study as opposed to the skin, that would receive the maximal radiation dose. The dose received by the volume under study in the sweeping beam

technique is 1/3 times the dose given to the skin in the fixed beam case given by Equation (13) which is below 1 rad for the considered case.

One might try to find the photon energy which minimizes the dose for the given statistical accuracy. The result is similar to the result of an equivalent analysis in X-ray reconstructive tomography [33].

The dose has a very broad minimum for incident photon energies above 80 keV. Above this energy the increase in absorbed energy per photon in Equation (19) is compensated by a decrease in attenuation factors in Equation (18).

D. Exposure Time

We have seen that for a good precision Compton profile analysis we need about 2.6×10^9 incident photons. Photons have to be parallel within half of degree in a circular area of 3 mm diameter. The simplest way to prepare such a photon beam is by collimating a practically point-like radioactive source 17 cm away. The resulting photon beam contains only 2×10^{-5} of all photons emitted in all directions from the radioactive source. If we want to have an exposure time of 10 minutes, the source intensity has to be $2.6 \times 10^9/(2 \times 10^{-5} \times 600 \text{ sec}) = 2.1 \times 10^{11}$/sec or about 6 Curie. A shorter exposure time can be achieved with a more intense radioactive source.

The rate of events analyzed by the detector is only 1.7 kHz or about 1% of the rate limit due to the peaking time of 4 μs.

The problems connected with the multiple scattering inside the human body will not be discussed here in detail. The problem is mathematically complicated and usually requires the use of a Monte Carlo method [14]. For an actual measurement of Compton profiles the direct measurement of the effect of multiple scattering is preferable. It will always be the case in the proposed application. It is our "educated estimate" that the multiple scattering will limit the method to cases when the sample under investigation is about one attenuation length or 6cm deep within the human body.

Conclusion

A new method to analyze the elemental composition of tissues located deep inside the human body without having to physically access them was proposed. One of its major applications is the detection of density and chemical changes in coronary and cerebral arteries due to arteriosclerosis.

The method is based on well known properties of the Compton profiles of different elements. A high resolution germanium detector of large area is needed to perform the analysis in vivo without submitting patients to an excessive radiation dose.

A recent development in the field of semiconductor detectors, based on new concepts of charge transport, makes the realization of such a detector possible. The test results of similar detectors built by the authors confirms the validity of these new concepts.

In this proposal we have presented a thorough formulation of the concepts and we have elaborated all the technical aspects important to the physical realization of the apparatus.

References

1. G.N. Hounsfield, (1968) British Provisional Patent No. 1283915. G.N. Hounsfield, British J. Radiol., 46, 1016.
2. R.A. Brooks and G. DiChiro, Phys. Med. Biol., 21 (1976), 689.
3. P.C. Lauterbur, Pure Appl. Chem., 40, 149.
4. M.J. Day, Phys. Med. Biol., 29, (1984), 121.
5. D.F. Jackson and D.J. Hawkes, Physics Reports, 70, (1981), 169.
6. A.H. Compton, Phys. Rev., 21, (1923), 483.
7. J.W.M. DuMond, Phys. Rev., 33, (1929), 643.
8. P. Eisenberger and P.M. Platzman, Phys. Rev. A2, (1970), 415.
9. P. Eisenberger and W.A. Reed, Phys. Rev. B9, (1974), 3237.
10. R. Ribberfors, Phys. Rev. B12, (1975), 2067.
11. W. Weyrich, P. Pattison and B.G Williams, Chem. Phys. 41, (1979), 271.
12. M. Cooper, Adv. Phys., 20, (1971), 453.
13. I.R. Epstein, Acc. Chem. Research, 6, (1973), 145.
14. B.J. Williams ed., Compton Scattering. The investigation of electron momentum distributions. (McGraw-Hill, 1977).
15. M.J. Cooper, Contemp. Phys., 18, (1977), 489.
16. F. Biggs et al., Atomic Data and Nuclear Data Tables, 16, (1975), 201.
17. W.A. Reed and P. Eisenberger, Phys. Rev. B6, (1972), 4596.
18. Chapter 7 in Reference (14).

References (cont'd.)

19. P. Eisenberger and W.A. Reed, Phys. Rev. A5, (1972), 2065.

20. E. Gatti and P. Rehak, Nucl. Instr. Meth. 225, (1984), 608.

21. E. Gatti, P. Rehak and J.T. Walton, Nucl. Instr. Meth. 226. (1984), 129.

22. E. Gatti et al., To be published in Nucl. Instr. Meth.

23. G.F. Knoll, Radiation Detection and Measurement, John Wiley, New York 1979, p. 373.

24. P. Luke et al., to be published in IEEE Transactions on Nuclear Science, NS-32 (1985).

25. V. Radeka, IEEE Trans. Nucl. Sci. NS-15, (1968), 455.

26. F.S. Goulding, Nucl. Instr. Meth. 100, (1972), 493.

27. S. Manninen and T. Paakkari, Nucl. Instr. Meth. 155, (1978), 115.

28. P. Pattison and J.R. Schneider, Nucl. Instr. Meth. 158, (1979), 145.

29. U. Bonse et al., J. Appl. Cryst. 12, (1979), 432.

30. M.J. Cooper et al., J. Phys. E 11, (1978), 1145.

31. E. Storm and H.I. Israel, Nucl. Data Table A7, (1970), 590.

32. H .W. Kraner, IEEE Trans. Nucl. Sci. NS-29, (1982), 1088.

33. R.A. Brooks and G. DiChiro, Medical Physics 3, (1976), 237.

34. P.G. Lale, Phys. Med. Biol., 4, (1959) 159.

35. R.L. Clarke, Atomic Energy of Canada Rept. No. 2270 (1965).

36. J.J. Battista and M.J. Bronskill, Phys. Med. Biol., 26, (1981), 81.

37. J.M. Jauch and F. Rohrlich, The Theory of Photons and Electrons. Addison-Wesley, Cambridge, Mass., 1955.

Figure Captions

1.a) Apparatus to provide elemental analysis of a selected small volume inside the patient's body. A well collimated beam of monoenergetic γ-rays (photons) penetrates the patient's head and crosses the selected volume under study. The photons scattered backwards from the volume are detected and measured in a germanium detector of high resolution. Collimators in front of the detector stop the background radiation from reaching the detector. The upper part shows the top view, the lower part the side view.

b) Lamellas of two collimators to detect photons coming only from a selected volume. The first collimator allows photons scattered along the collimator axis only to reach the detector. The second collimator (shown in an axial cross section) further selects a specific point on the collimator's axis.

2.a) Kinematics of the Compton scattering on a free electron at rest. ω_1, ω_2 are the initial and final photon energies, respectively.

b) Kinematics of the Compton scattering in the impulse approximation. The z-axis is defined for each scattering event as being parallel and of opposite orientation to the photon momentum transfer.

3. Energy spectrum of photons scattered into a well defined angle θ. The energy of the primary photon ω_1 is shown. The real spectrum has a Gaussian-like shape centered around the value ω_2 given by Equation (1).

Figure Captions (cont'd.)

4. (From Ref. [8]) Comparison of experimental Compton profile with that calculated by the IA. The areas under the two distributions were normalized to 2 which is the number of electrons per atom in helium. The solid line is the experimental profile, the calculated profile is the dotted line. For definition of atomic unit of momentum see Appendix II.

5. Calculated Compton profiles J(q) for atomic hydrogen, carbon and sodium normalized to 1 electron. The curves were drawn according to the Tables in Ref. [16].

6. (From Ref. [17].) Comparison of the Compton profiles for atomic carbon (squares); ethane gas (open circles); and diamond dust (triangles). The experimental errors are smaller than the size of the symbols.

7. Apparatus to study the elemental composition of a tomographical plane. Photons scattered around 90° are detected. a) Perspective view; b) View parallel to the incident beam. The lamellas of the collimator are well visible; c) The geometry of scattering and detection.

8. Klein-Nishina differential cross-section for incident photons of energy ω_1 = 159 keV.

9.a) Perspective view (not to scale) of the semiconductor drift detector. The motion of electrons within the detector is shown.

b) Potential energy of electrons within the detector. Electronsmove downwards to minimize their potential energy.

F' ure Captions (cont'd.)

10. Position resolution obtained in a recently produced silicon drift detector. Note the scale in μm.

11. Germanium detector with a built-in transverse drift field. The small capacitance anode is at the left edge of the detector connected to a preamplifier.

12. (From Ref. [27]) Broadening of the Compton peak as a function of the incident photon energy. The dotted line shows the contribution from the ener y resolution of the detector. Solid lines are the contributions from an angular error of 2 degrees (FWHM) at the different values of the scattering angle θ. The energies typically used for Compton experiments are indicated by arrows.

13. Contribution of the finite beam size to the angular uncertainty of the measurement. d - is the diameter of the beam when it reaches the volume under study; h is the height of the volume element.

Pavel Rehak

Appendices to the Proposal for a New Tomographic Device Providing Information on the Chemical Properties of a Body Section

APPENDIX I.

Statistical Accuracy of the Compton Profile Decomposition into "Basic Profiles"

The idea to perform the elemental analysis of a region of tissue located deep inside the human body was described in the proposal. The proposed method is based on the precise measurement of the Compton profile. In principle each chemical element has its own Compton profile and the decomposition of the measured profile into a sum of Compton profiles of individual elements gives the required elemental composition.

Here we will show how well, that is, with what accuracy the decomposition can be done. The problem can be appreciated by looking at Fig. 5 of the proposal where Compton profiles of hydrogen, carbon and sodium are shown. In contrast to a standard X-ray fluorescence spectroscopy, where peaks belonging to the individual elements are separated on the x-axis, the Compton profiles of all elements are situated at the same location. The differences are only

in the shape of the Compton profile of the individual elements. The decomposition of a measured Compton profile is less constrained than the analog analysis of the individual peaks in a conventional X-ray spectroscopy. We may expect the Compton profile method to be less accurate than the spectroscopic methods.

(At this point one may question the practicality of the Compton profile method. The answer is quite simple. The energy of the fluorescent X-rays emitted by the common elements in the human tissue is so low that this radiation is absorbed inside the human body after traversing only a few μm. The X-ray fluorescence method works very well indeed but only for a surface analyses. To penetrate through the body tissue and carry the information from inside the body the photon energy has to be above the energy range of X-ray spectroscopy.)

We are going to describe a decomposition of measured Compton profile into the basic Compton profiles by the least squares method. It can be shown that in our case the least squares method is equivalent to the maximum likelihood method which means that we are treating our problem in the best way in the statistical sense.

Similar to Section IV of the proposal, this appendix will derive the statistical accuracy of the elemental composition of a selected small region inside the human body. A reader not interested in mathematical details may wish to skip part A and go to the clinical example.

A. Mathematical Method

Let us denote the measured Compton profile by $M(q)$. This profile $M(q)$ obtained during the exposure, is stored in the computer memory in the form of a histogram. The k-th bin of the histogram contains $M(q_k)\cdot\Delta q$ counts which tells us how many times a Compton scattering on an electron with the value of z-component of momentum between q_k and $q_k + \Delta q$ occurred. We denote the Compton profile of the i-th individual element $J_i(q)$, i=1,2...p, where p is the total number of elements from which the profile is composed. In the spirit of the decomposition we would like to satisfy the following n equations for each histogram bin k

$$[M(q_k) - b(q_k)] \cdot \Delta q - \sum_{i=1}^{p} N_i \cdot J_i(q_k) \cdot \Delta q = 0 \qquad (A1)$$

$$k=1,2,3,\ldots n$$

where $b(q_k)\cdot\Delta q$ is the expected background in the k-th bin, N_i is the unknown electron density of the i-th element in tissue, Δq is the bin width, n is the total number of bins, and $M(q_k)$ and $J_i(q_k)$ were defined previously. Eq. (A1) states that the measured spectrum $M(q_k)$ after correction for background is equal to the weighted sum of individual Compton profiles at each bin of the histogram. There are generally many more bins (n) in the histogram than the number of the element (p). The condition (A1) is too restrictive and has to be replaced by its statistical equivalent.

$$S = \sum_{k=1}^{n} [M(q_k) - b(q_k) - \sum_{i=1} N_i J_i(q_k)]^2 \Delta q^2 / \sigma_k^2 = \text{minimum} \quad \text{(A2)}$$

$$\text{where } \sigma_k^2 = \sum_{i=1}^{p} N_i \cdot J_i(q_k) \cdot \Delta q + b(q_k) \cdot \Delta q \quad \text{(A3)}$$

Eq. (A2) states that the unknown electron densities N_i, i=1,2,3 ...p, must be chosen in such a way that the weighted sum of squares of the deviations from zero (called the residuals), as imposed by Eq. (A1), is minimized. The weight of each bin is inversely proportional to the statistical error in that bin.

Eq. (A2) can be written in a matrix notation

$$S = R^T \cdot W \cdot R \quad \text{(A4)}$$

where R is an (nx1) column vector with the k-th element

$$R_k = [M(q_k) - b(q_k)] \cdot \Delta q - \sum_{i=1}^{p} N_i \cdot J_i(q_k) \cdot \Delta q \quad \text{(A5)}$$

R^T -is its transposed (1xn) row vector and W is the weight (nxn) matrix. In our case the weight matrix is diagonal with $W_{kk} = 1/\sigma_k^2$, where σ_k^2 is given by (A3). We can use the matrix notation again to rewrite the sum over the index i in Eq. (A5). The residual vector R can be thus written as

$$R = [M - b] - J \cdot N \quad \text{(A6)}$$

where M and b are (nx1) column vectors of the measured histogram and background, respectively. N is an (px1) column vector of unknown

electron densities N_i and J is the (nxp) matrix of the basic Compton profiles.

The expression for the weighted sum of squares S given by Eq. (A4) is now written in the standard form found in books dealing with Statistics and Estimation theory. Eq. (A4) is practically identical to the Eq. 8.12 of Ref. [A1]. The solution, that is, the vector N which minimizes the weighted sum S is (Eq. 8.13 of the same Reference).

$$N = (J^T W J)^{-1} \cdot J^T W \cdot (M-b) \qquad (A7)$$

Eq. (A7) was obtained by equating to zero all partial derivatives of S relative to the vector of unknown densities N . To linearize the problem we have neglected a weak dependence of W on the N. This approximation is equivalent to a slightly different definition of the σ_k^2 in Eq. (A2). If we substitute (A1) into σ_k^2 we obtain

$$\sigma_k^2 = M(q_k) \cdot \Delta q \qquad (A8)$$

Eq. (A8) instead of Eq. (A2) is often used to define the weight matrix W.

From the Theory of Estimators we know that the Eq. (A7) gives the unknown densities in an unbiased way. The accuracy in which the densities were obtained from the measured histogram is given by the variance matrix of the densities.

In our case the variance matrix is (Ref. A1, Eq. 8.25)

$$\text{var}(N) = (J^T \cdot W \cdot J)^{-1} \qquad (A9)$$

To gain insight into the meanings of Eq. (A9) let us consider the simplest case of the measured Compton profile to be decomposed

into a sum of two profiles J_1 and J_2. We have only two unknown electron densities N_1 and N_2 and the matrix manipulation is relatively simple. The elements of the inverse variance matrix given by Eq. (A9) are thus reduced to

$$[\mathrm{var}(N)^{-1}]_{\ell,m} = \sum_{k=1}^{n} \frac{J_\ell(q_k) \cdot J_m(q_k) \cdot \Delta q^2}{(N_1 \cdot J_1(q_k) + N_2 J_2(q_k) + b(q_k))\Delta q} \qquad \text{(A10)}$$

If the bin width is small compared with the width of the profile, the sum in Eq. 10 can be replaced by the integral and we can write

$$[\mathrm{var}(N)^{-1}]_{\ell,m} = \int_{-\infty}^{\infty} \frac{J_\ell(q) \cdot J_m(q) \cdot dq}{N_1 J_1(q) + N_2 J_2(q) + b(q)} \cdot \qquad \text{(A11)}$$

To simplify the mathematics even further we neglect the background b(q) in the denomination of (A11) and invert the matrix equation. The variance matrix can now be written in the following explicit form

$$(\mathrm{var}N) = \frac{N_{TOT}}{1-a} \begin{pmatrix} \alpha_1(1-\alpha_1 a) & -a\alpha_1\alpha_2 \\ -a\alpha_1\alpha_2 & \alpha_2(1-\alpha_2 a) \end{pmatrix} \qquad \text{(A12)}$$

$$\text{where } a = \int_{-\infty}^{\infty} \frac{J_1(q)J_2(1)\, dq}{\alpha_1 J_1(q) + \alpha_2 J_2(q)} \qquad \text{(A13)}$$

$$\text{and } N_{TOT} = N_1 + N_2; \quad \alpha_1 = \frac{N_1}{N_{TOT}} \; ; \quad \alpha_2 = \frac{N_2}{N_{TOT}} \qquad \text{(A14)}$$

The diagonal elements of the variance matrix are loosely called the errors of the corresponding densities.

The quantity as defined by (A13) is the quantitative expression for the loss of the precision of the Compton profile method relative to the ideal fluorescence spectroscopy method. For two distinct peaks in a spectroscopy, there is no overlap of $J_1(q)$ and $J_2(q)$ and a equals to zero. The zero value of the parameter a gives the smallest statistical error with a given total count N_{TOT}.

At the other extreme, if the profile J_1 is the same as the profile J_2 the parameter a is equal to zero and the errors go to infinity. We should expect this result; the decomposition of anything into two identical profiles is undefined and can be done in an arbitrary way.

The value of the parameter a for Compton profiles is between these two extremes.

B. Clinical Example

We consider a possible application of the Compton profile method to the study of osteoporosis. Let us assume that the problem is to determine the concentration of the bone salt in the bone tissue. We assume that the Compton profile of the bone salt - hydroxyapatite is the weighted sum of the profiles of individual elements forming the hydroxyapatite $\left(3[Ca_3(PO_4)_2] \cdot Ca(OH)_2\right)$ [16]. In this model we neglect all effects of the chemical bonds of the salt.

The Compton profile of the bone tissue is approximated by that of the water and also here we neglect all chemical effects.

Fig. A1 shows normalized Compton profiles of water and hydroxyapatite. Two curves are associated with each substance. One is the ideal profile, the second profile is the convolution of the first one with the realistic resolution of the detection system. These are the experimentally observable profiles. Moreover, in Fig. 1A there are two lines indicating the amount of background relative to the height of the profiles. The lower line indicates the level of background from Ref. [19] of the proposal. This level might be too optimistic. The second line indicates a background level 3 times higher than the reported level. We believe that this second line corresponds to an overestimation of the background in a real exposure.

Fig. A2 shows the accuracy of the decomposition of the measured Compton profile into basic profiles, that is, it shows the accuracy of the determination of the bone composition. The plotted errors are for 10^6 detected photons as was assumed in Section IV of the proposal.

The lowest curve shows the error in the determination of the hydroxyapatite content in the ideal case of the perfect resolution and with no background. The parameter a defined by (A13) is roughly

.97 depending slightly on the hydroxyapatite concentration. Division by (a-1) in (A12) means that the variance of the Compton profile is about 30 times larger (error is $\sqrt{30} = 5.5$ times larger) than it would be in the case of fully separated peaks in a spectroscopic analysis.

The second lowest curve shows the error in a less ideal case of the realistic system resolution (σ_q = .25 atomic units) with no background. The increase of the error compared to the ideal resolution curve is very small.

The remaining two curves show the errors in realistic cases of a given system resolution and backgrounds as shown in Fig. A1. A typical value is about 0.5% with only a slight dependence on the hydroxyapatite concentration.

C. Practical Conclusions

The above example demonstrates one possible use of the method for diagnosis. It may well be the case in many diseases that the sick tissue has a different Compton profile from the healthy tissue as a consequence of some chemical changes. These changes might be visible at .5% level by the proposed method while undetected by other methods.

The principles of the proposed method of Compton profiles are the fundamental laws of atomic physics and quantum electrodynamics. The rigorous foundation of the method should not, however, prevent

its application based on more empirical approaches. The capability to identify a diseased tissue by detecting a slight difference in the Compton profile relative to a healthy tissue is very useful. That we may not fully understand from the very first principles all the details of this difference does not affect the usefulness of the proposed method.

Reference:

A1. B.R. Martin, Statistics for Physicists. Academic Press, London and New York 1971.

APPENDIX II

Comments on Units and Notation used in the Proposal

Within the proposal the momentum, versus which all Compton profiles are plotted, is in atomic units of momentum. The definition of atomic units can be found in many books (Ref. [14], for example). To have a feeling for the size of the atomic unit of momentum it is convenient to remember that one photon of energy of 3.73 keV carries one atomic unit of momentum.

In Eq. (2) (page 7 of Proposal), the z-component of the momentum P_z of an electron on which the Compton scattering took place is proportional to the measured difference of the photon energy Δw. The constant of proportionality depends for a given energy of primary photons on the angle of the Compton scattering. This angle defines also the coordinate system, that is, the z-direction. The distribution of the z-components of momenta of the scattering electrons is the Compton profile $J(p_z)$.

The symbol $J(p_z)$ is used here in the mathematical sense as J being the function of the argument p_z. The name of the argument is not important. We can call it q, for example. The shape is always given by the functional dependence symbolized by the letter J. This notation is very convenient in our case. The electron

structure of the tissue has no preferred direction and all orientations of z-axis are equivalent. The method itself uses this isotropy to speed up the data collection and to decrease the radiation dose. The orientation of the z-axis is different for photons detected in different position of the detector. The argument p_z in the symbol of the Compton profile may be confusing, therefore a more neutral notation q was generally used in the sections of the Proposal dealing with the analysis of Compton profiles.

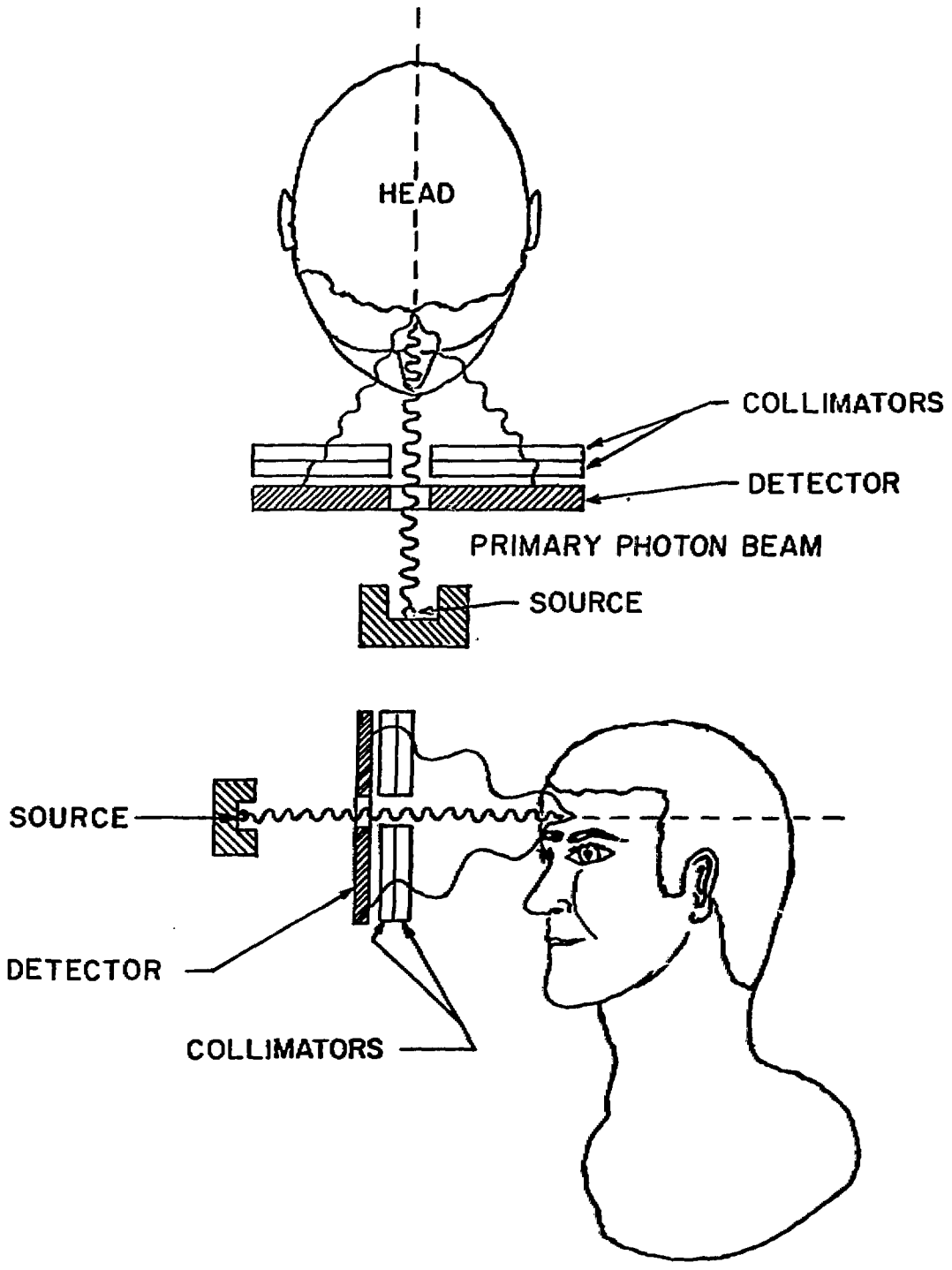
HEAD
COLLIMATORS
DETECTOR
PRIMARY PHOTON BEAM
SOURCE
SOURCE
DETECTOR
COLLIMATORS

Fig. 1a.

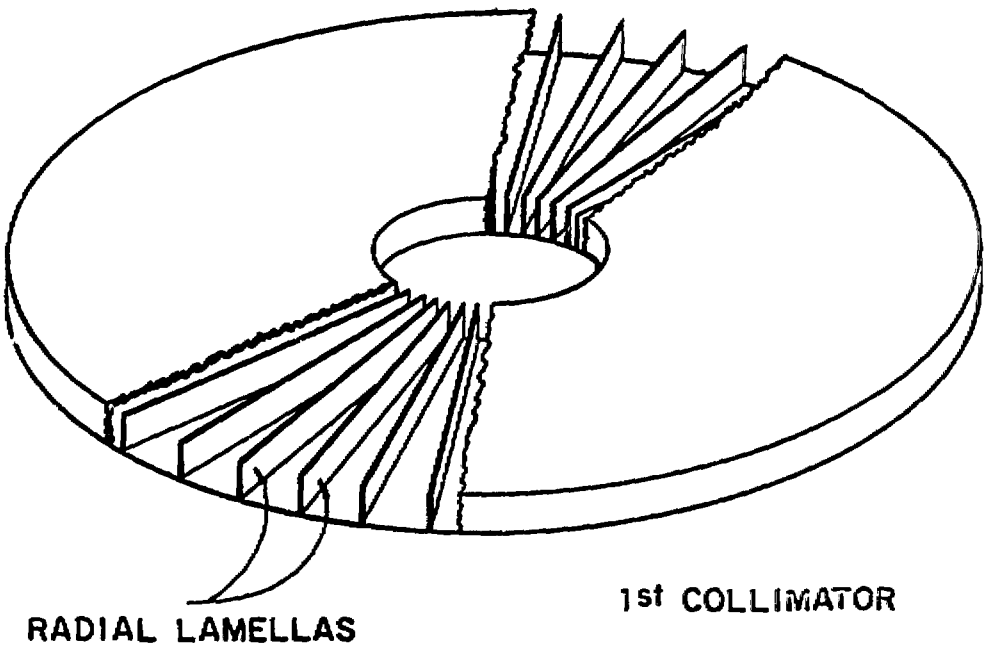

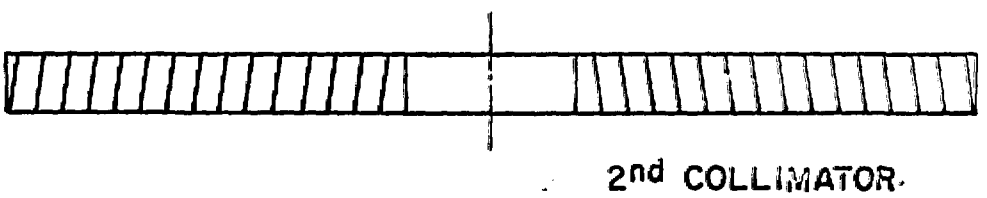

Fig. 1b.

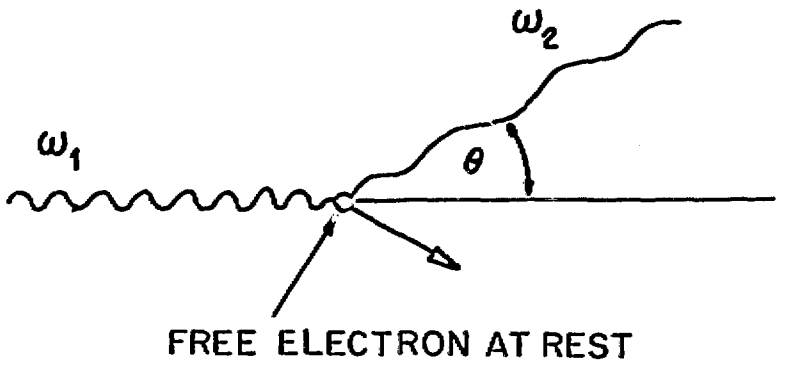

Fig. 2a

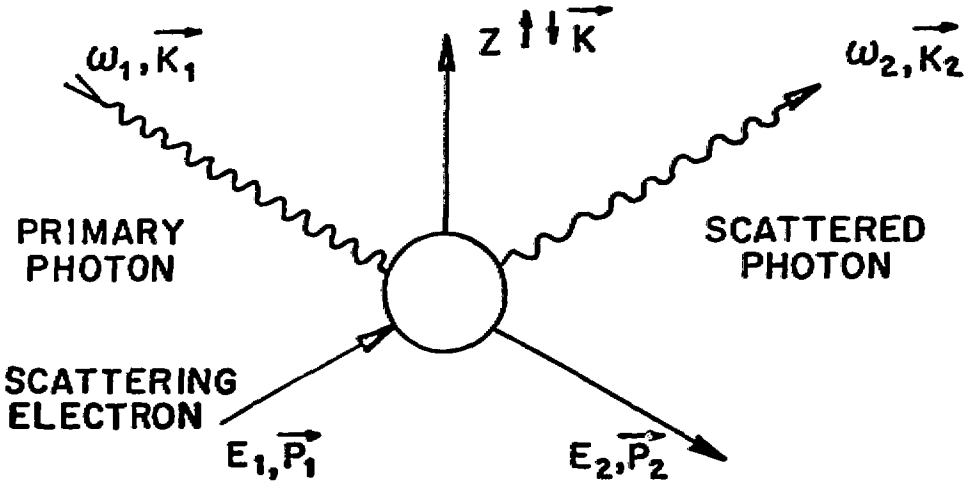

$\vec{k} = \vec{k_1} - \vec{k_2}$ — MOMENTUM TRANSFER

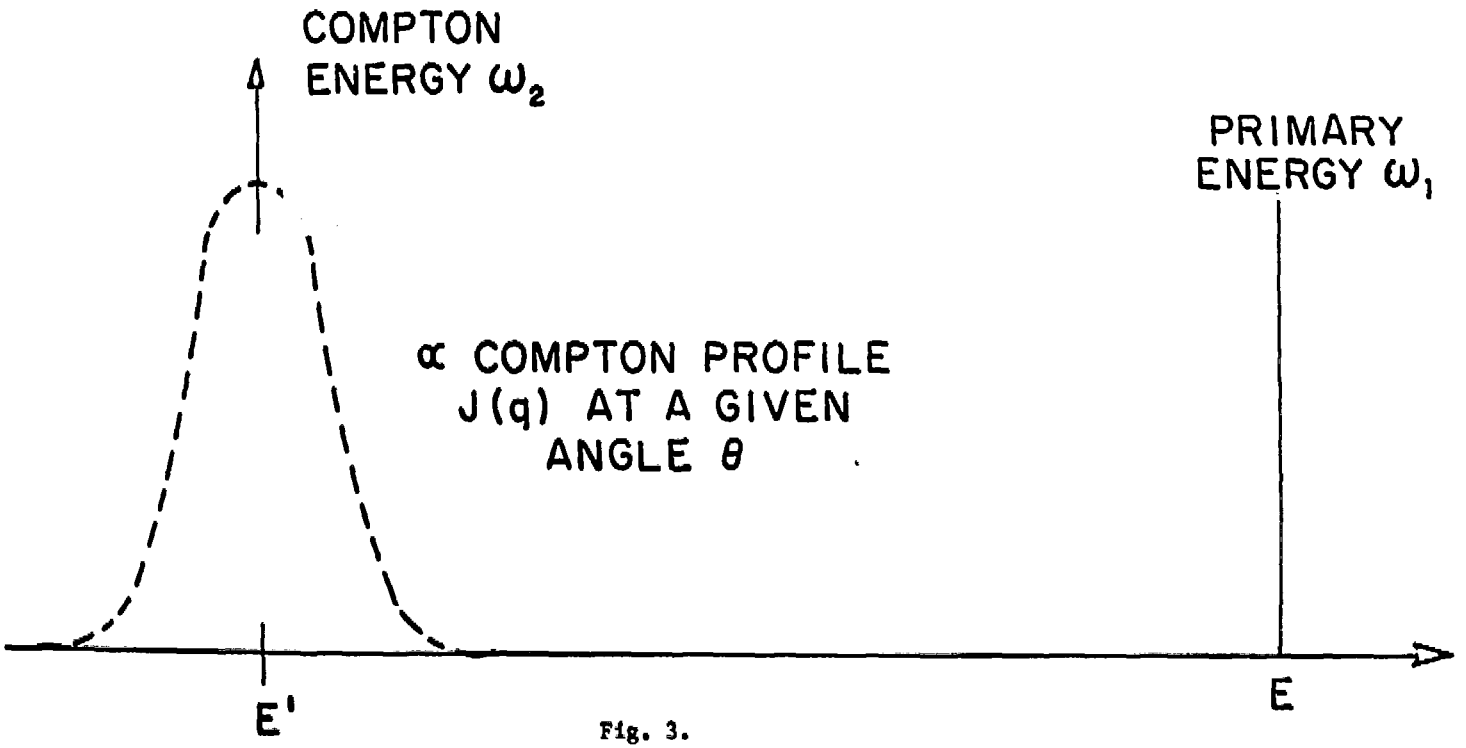
COMPTON
ENERGY ω_2
PRIMARY
ENERGY ω_1
$\propto$ COMPTON PROFILE
J(q) AT A GIVEN
ANGLE θ
E'
E

Fig. 3.

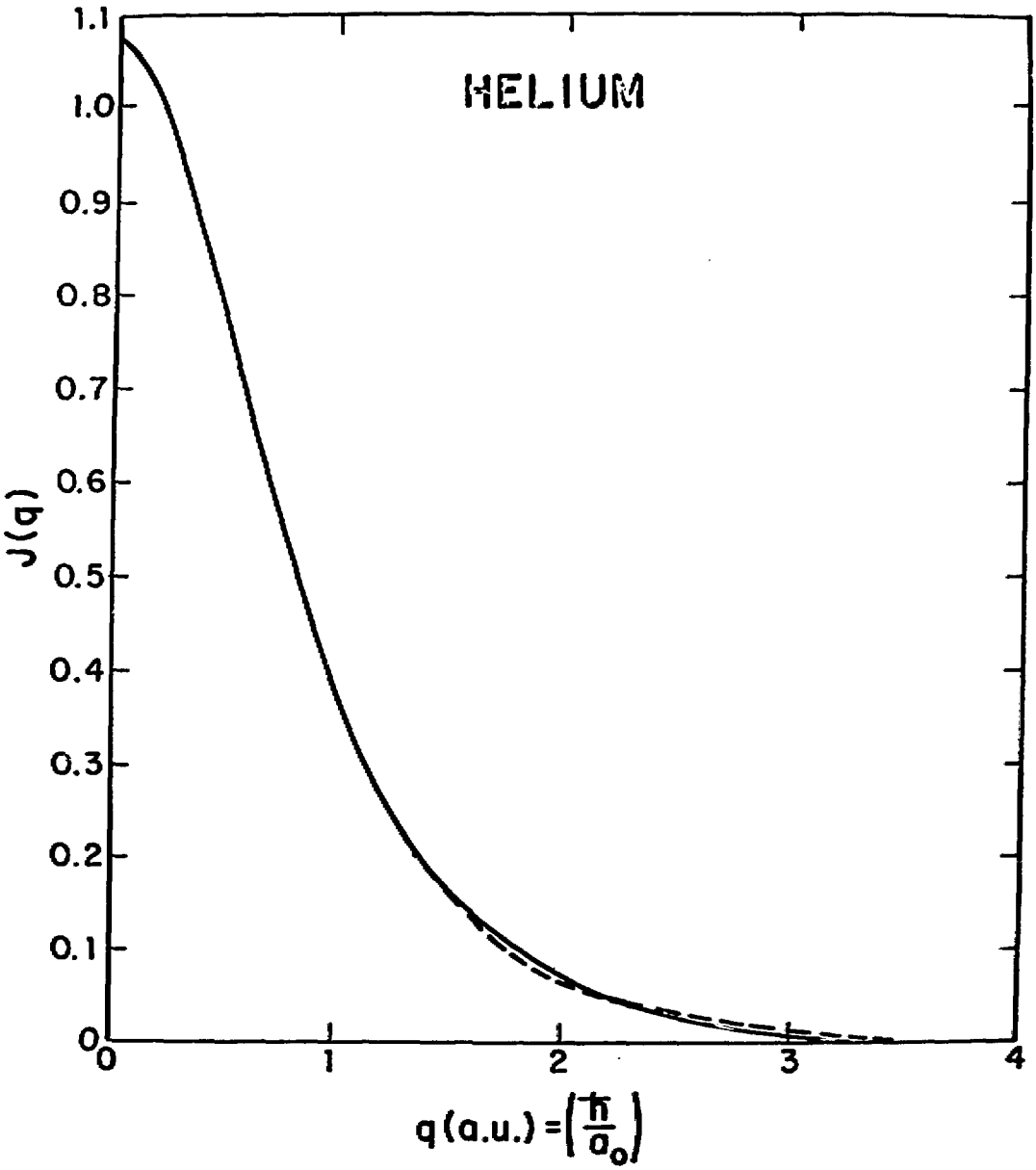

Fig. 4.

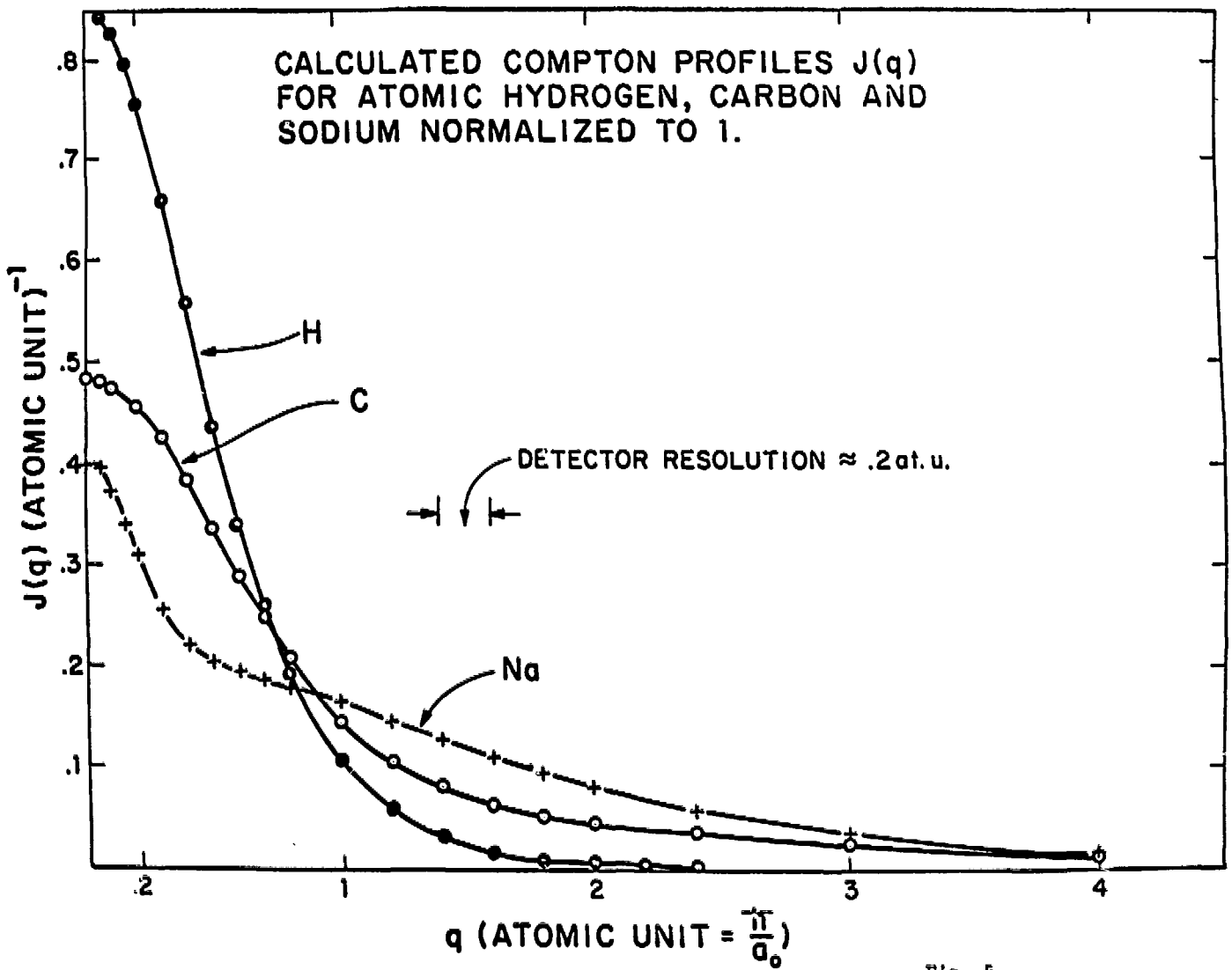
CALCULATED COMPTON PROFILES J(q)
FOR ATOMIC HYDROGEN, CARBON AND
SODIUM NORMALIZED TO 1.
J(q) (ATOMIC UNIT)$^{-1}$
.8
.7
.6
.5
.4
.3
.2
.1
H
C
Na
DETECTOR RESOLUTION ≈ .2 at. u.
.2
1
2
3
4
q (ATOMIC UNIT = $\frac{\hbar}{a_0}$)

Fig. 5.

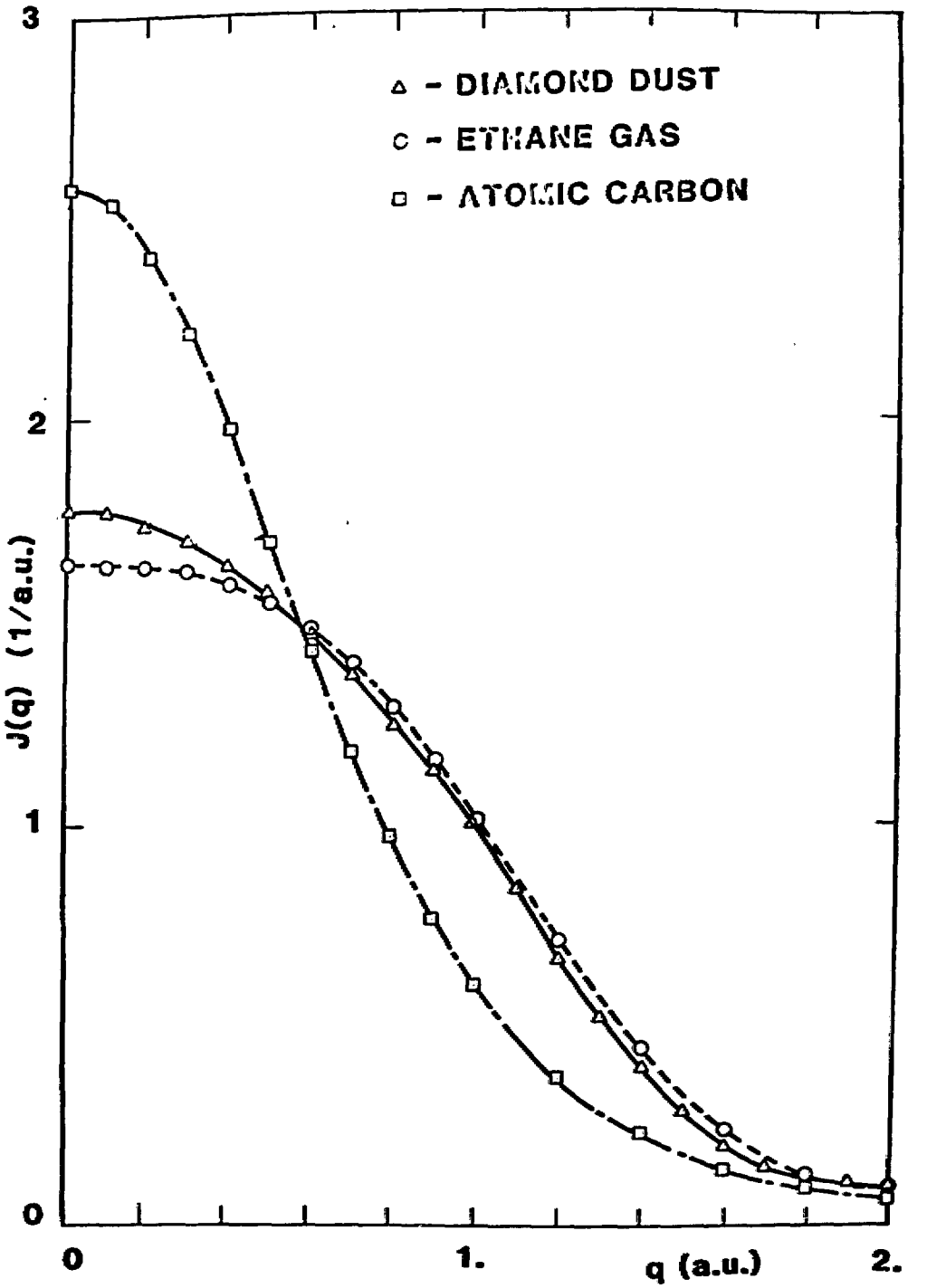

Fig. 6.

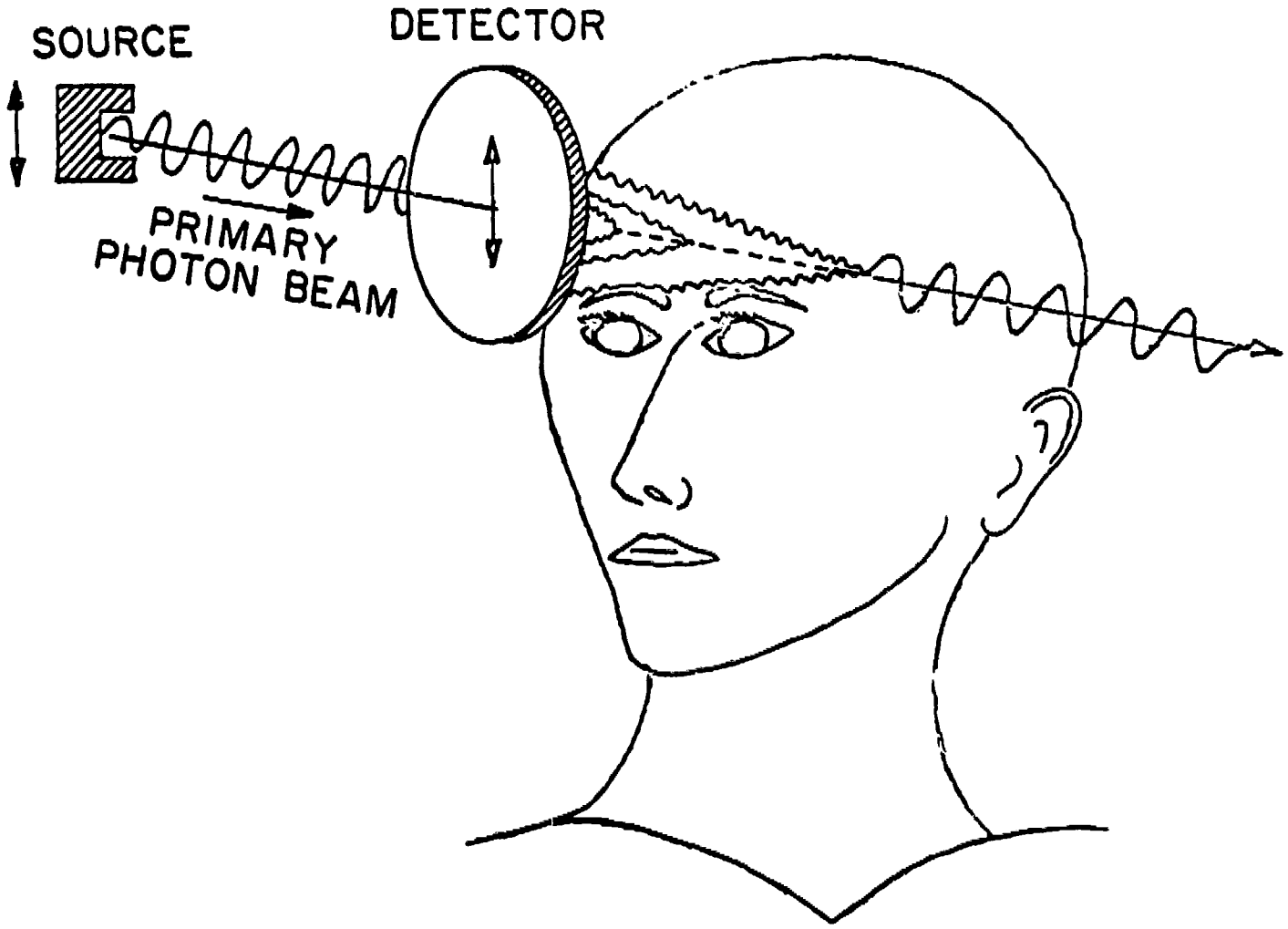

Fig. 7a.

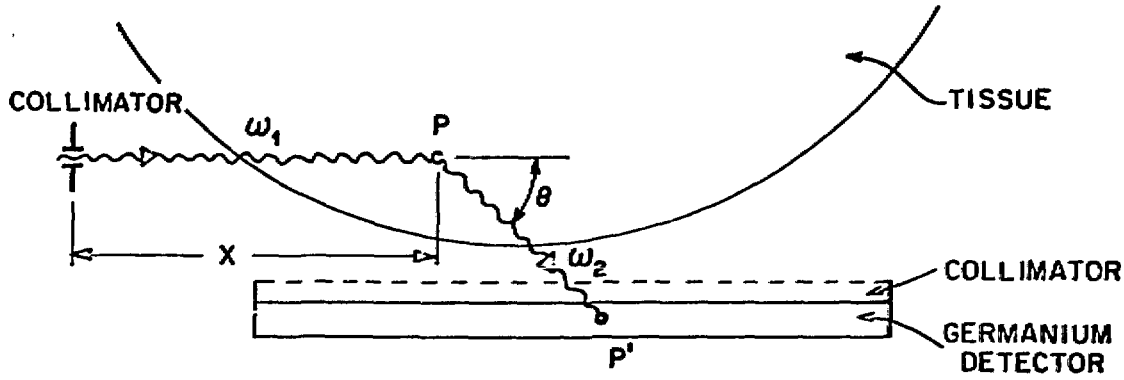
COLLIMATOR
ω_1
P
TISSUE
θ
X
ω_2
COLLIMATOR
GERMANIUM
DETECTOR
P'

Fig. 7c.

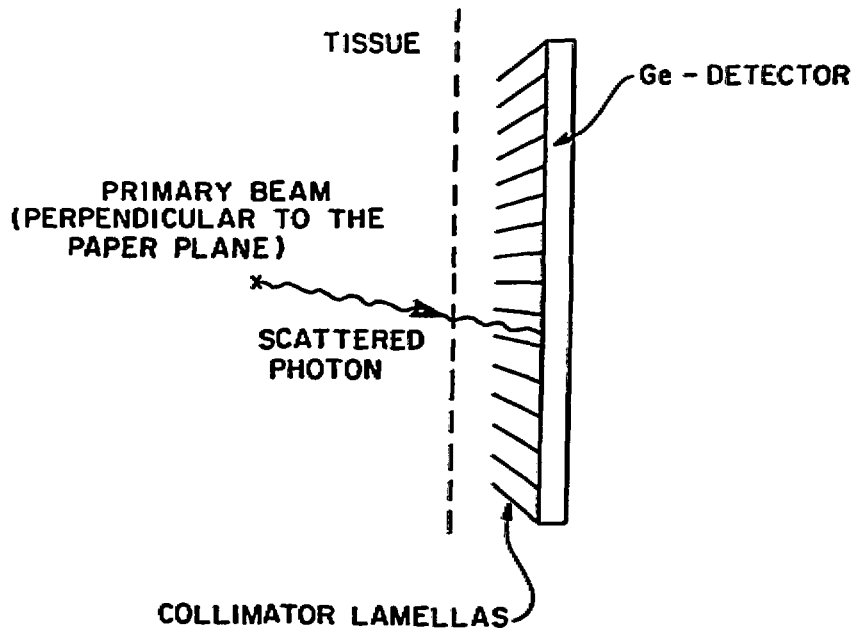
TISSUE
Ge - DETECTOR
PRIMARY BEAM
(PERPENDICULAR TO THE
PAPER PLANE)
SCATTERED
PHOTON
COLLIMATOR LAMELLAS

Fig. 7b.

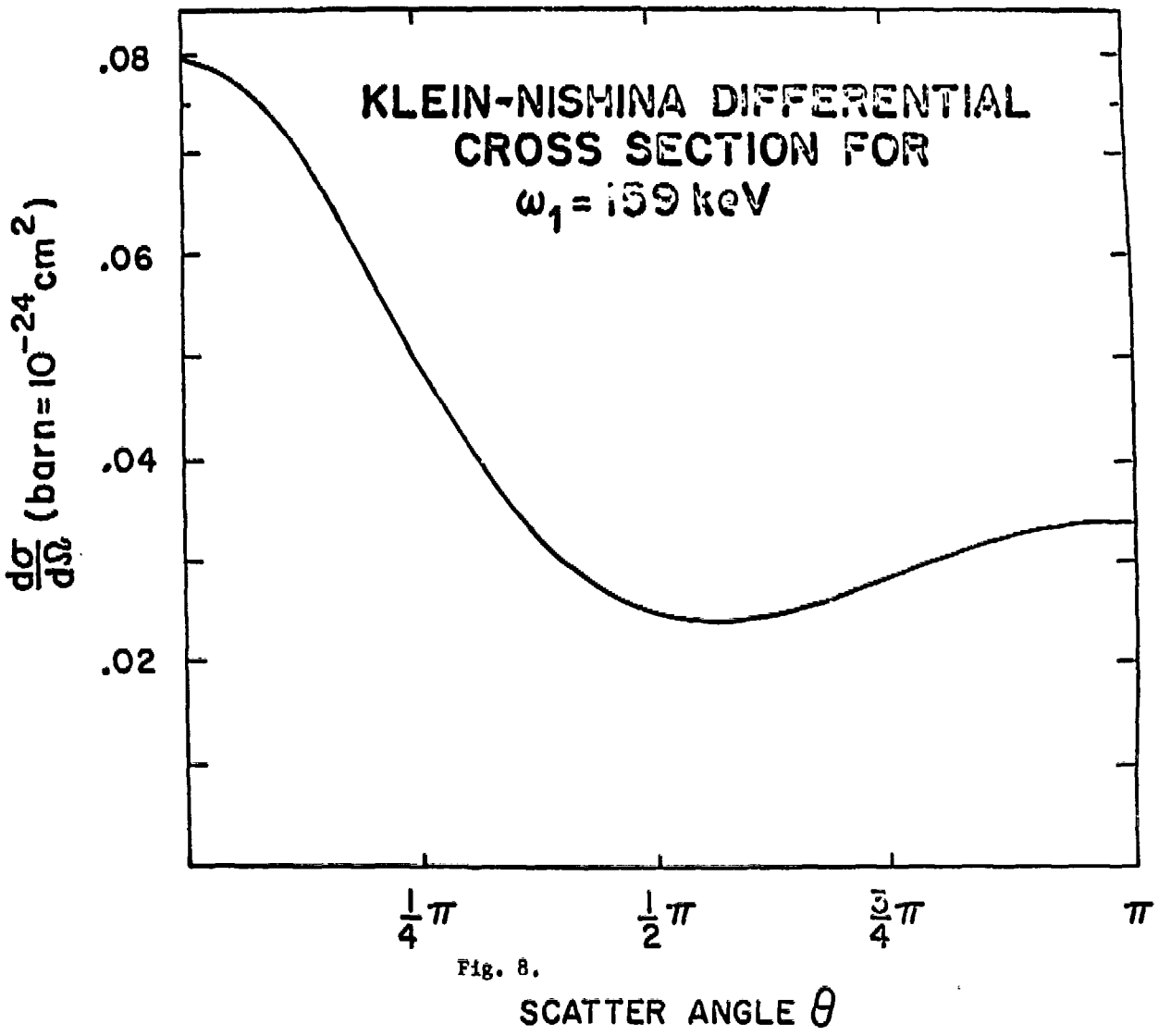
KLEIN-NISHINA DIFFERENTIAL
CROSS SECTION FOR
$\omega_1 = 159$ keV
$\frac{d\sigma}{d\Omega}$ (barn = 10^{-24} cm^2)
.08
.06
.04
.02
$\frac{1}{4}\pi$
$\frac{1}{2}\pi$
$\frac{3}{4}\pi$
π
SCATTER ANGLE θ

Fig. 8.

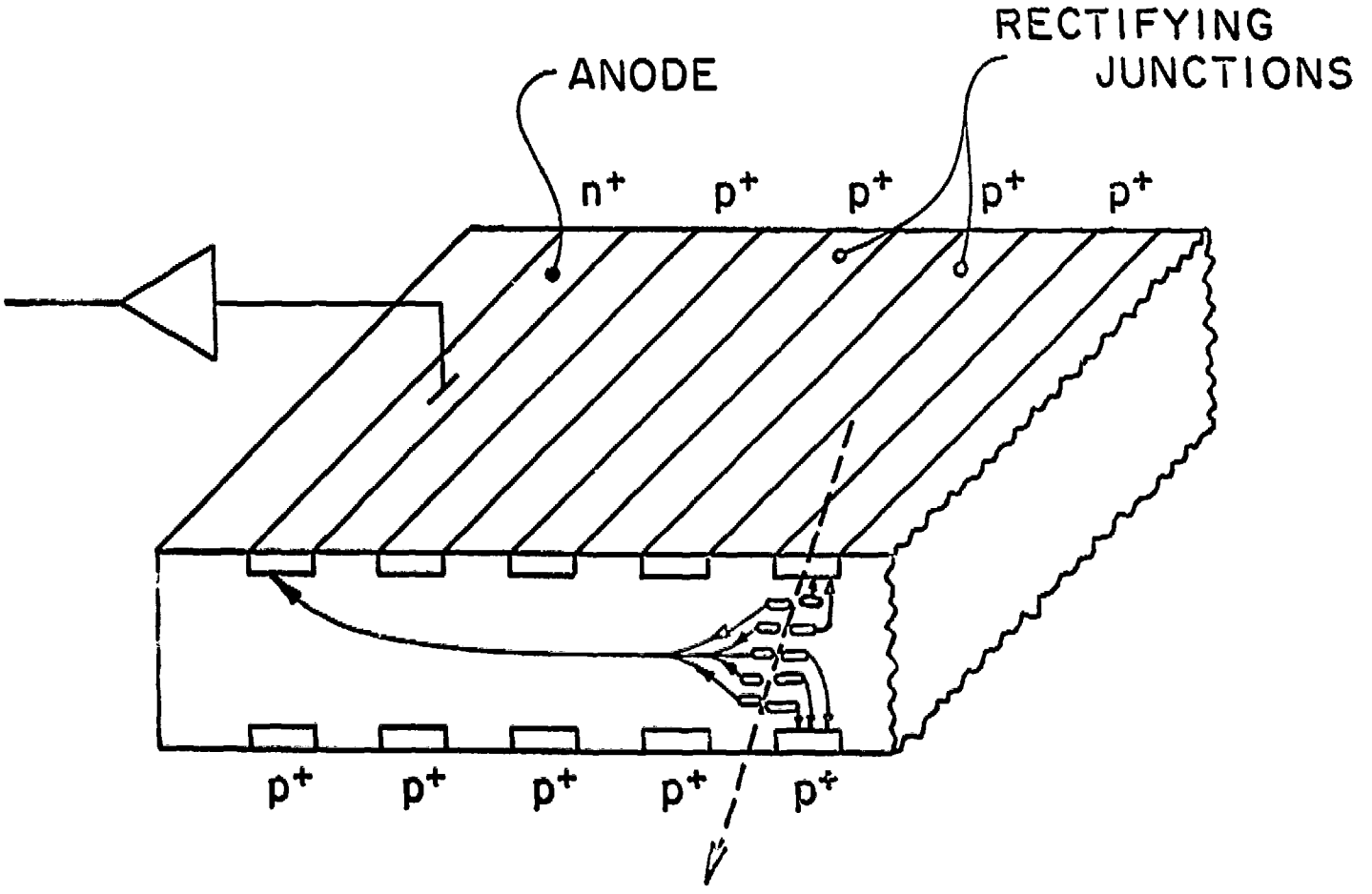

Fig. 9a.

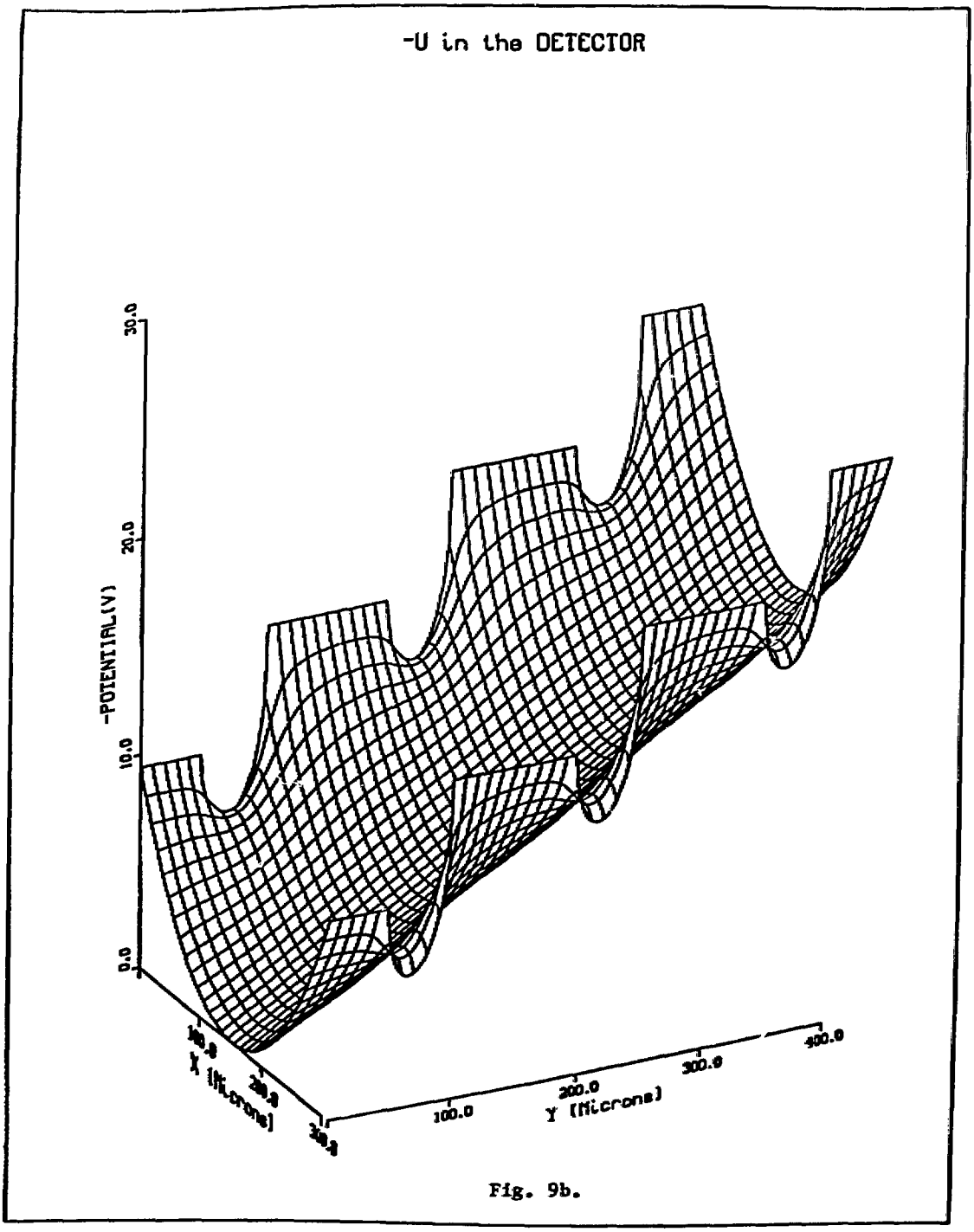
-U in the DETECTOR
-POTENTIAL(V)
30.0
20.0
10.0
0.0
100.0
200.0
300.0
400.0
Y (Microns)

Fig. 9b.

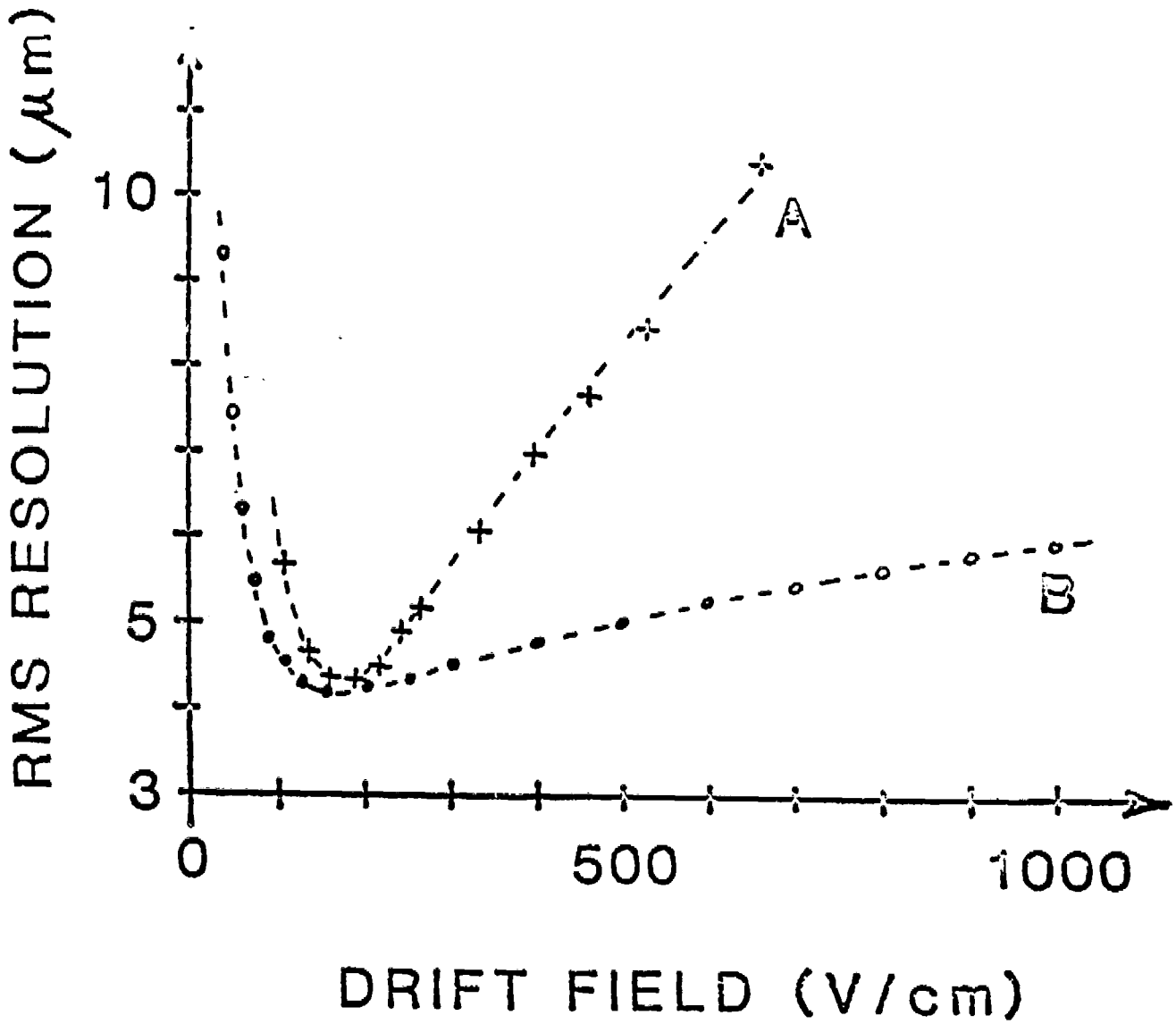

Fig. 10.

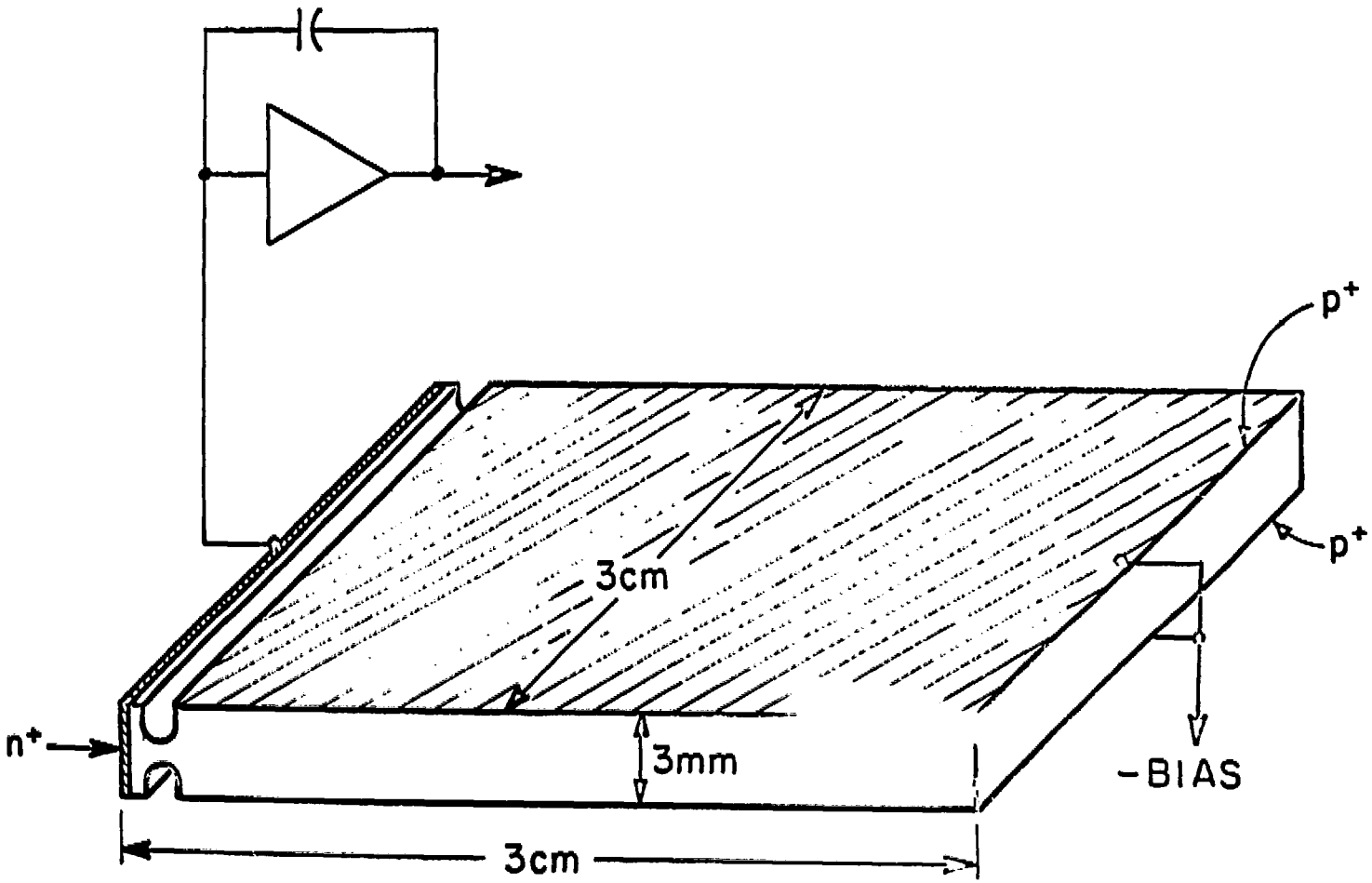

Fig. 11.

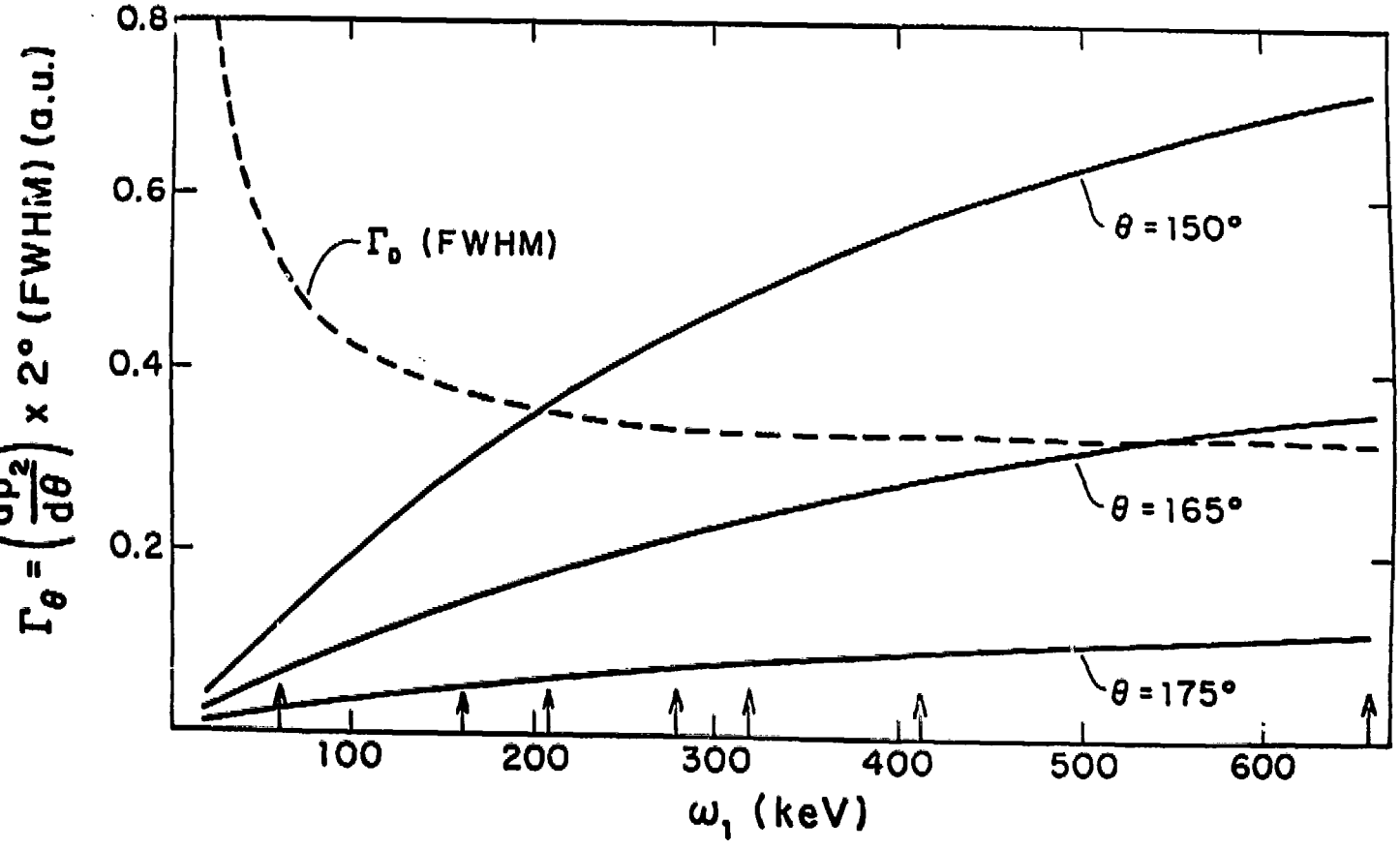
0.8
0.6
0.4
0.2
$\Gamma_\theta = \left(\frac{dp_2}{d\theta}\right) \times 2°$ (FWHM) (a.u.)
Γ_0 (FWHM)
$\theta = 150°$
$\theta = 165°$
$\theta = 175°$
100
200
300
400
500
600
ω_1 (keV)

Fif. 12.

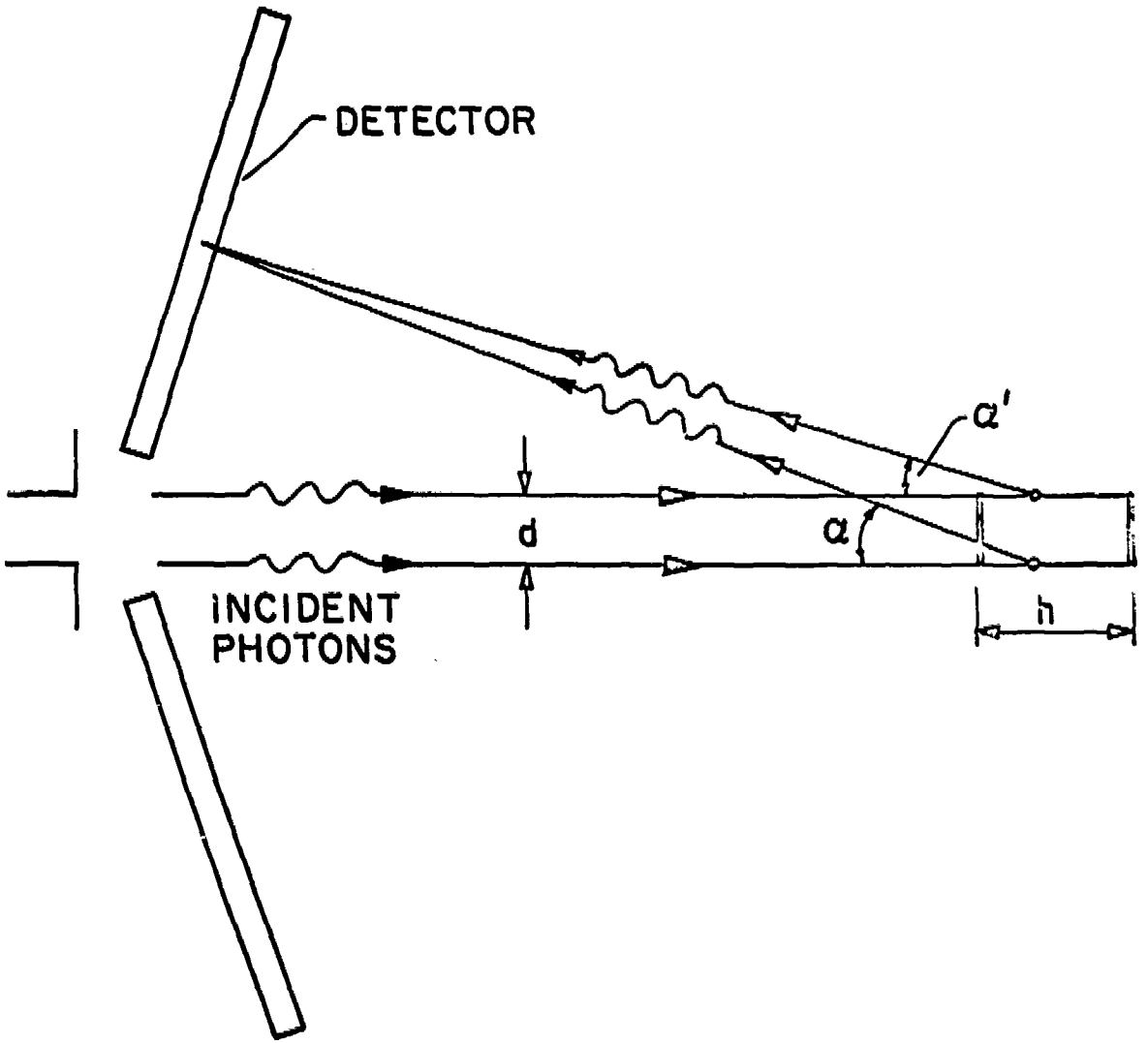

Fig. 13.

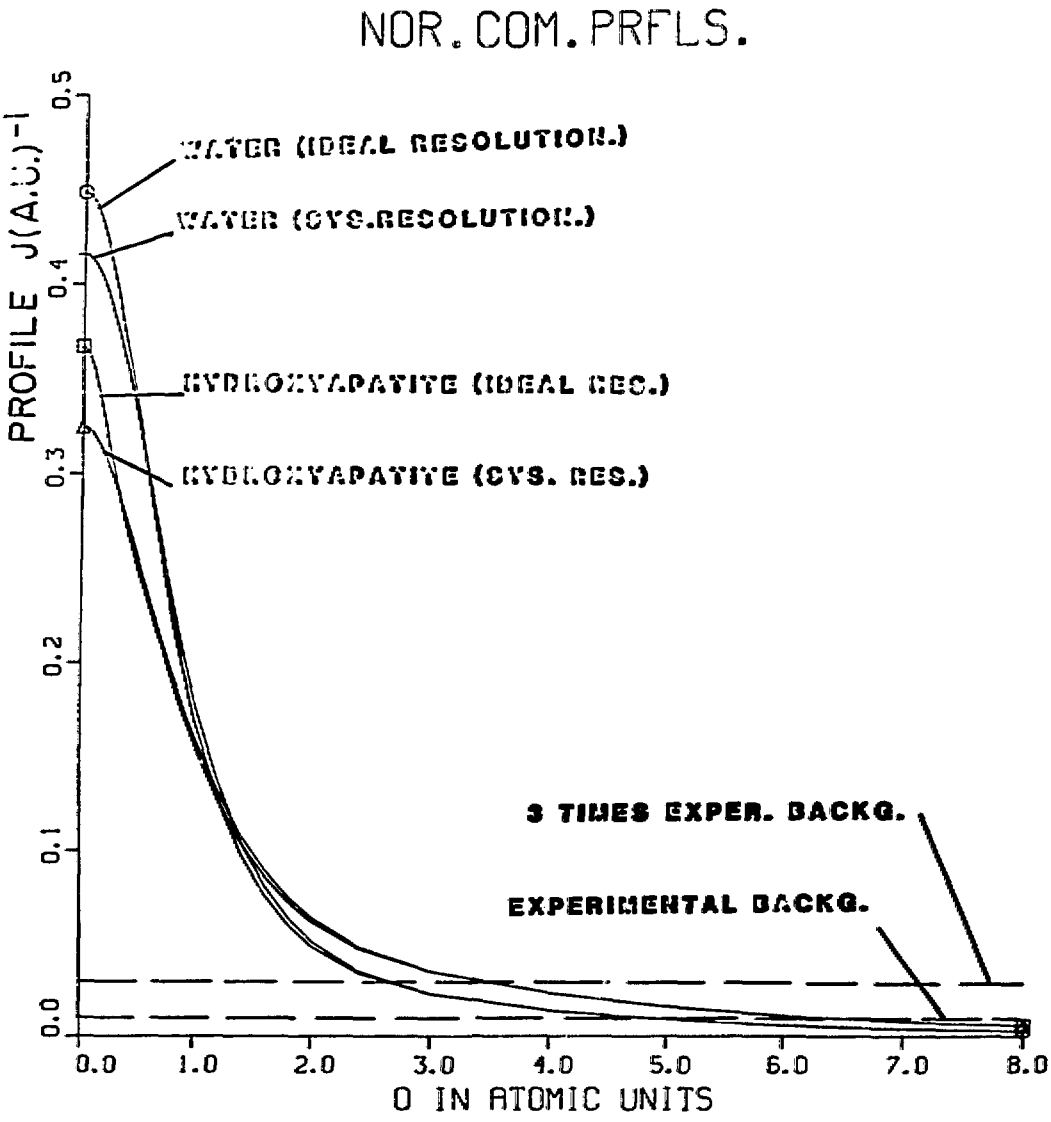
NOR. COM. PRFLS.
PROFILE J(A.U.)-1
0.0
0.1
0.2
0.3
0.4
0.5
WATER (IDEAL RESOLUTION.)
WATER (CYS.RESOLUTION.)
HYDROXYAPATITE (IDEAL RES.)
HYDROXYAPATITE (CYS. RES.)
3 TIMES EXPER. BACKG.
EXPERIMENTAL BACKG.
0.0
1.0
2.0
3.0
4.0
5.0
6.0
7.0
8.0
Q IN ATOMIC UNITS

Fig. A1.

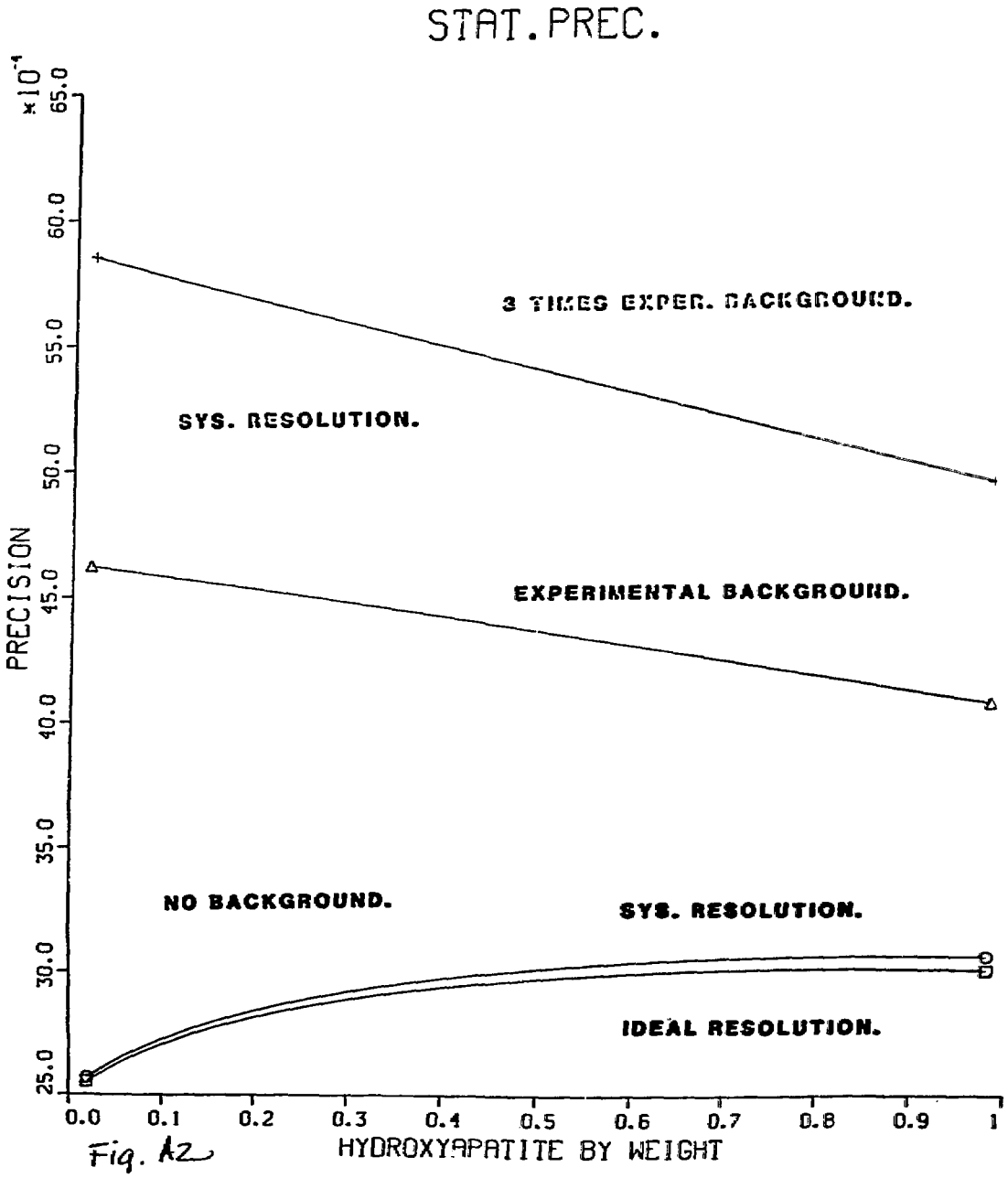

Fig. A2